# SYSTEM CONTROLS ON THE SOUTH TEXAS SAND SHEET

A Dissertation

by

CLIFTON PATRICK BARRINEAU

Submitted to the Office of Graduate and Professional Studies of
Texas A&M University
in partial fulfillment of the requirements for the degree of

DOCTOR OF PHILOSOPHY

| | |
|---|---|
| Chair of Committee, | Chris Houser |
| Committee Members, | Michael Bishop |
| | Mark Everett |
| | Vatche Tchakerian |
| Head of Department, | David Cairns |

May 2017

Major Subject: Geography

# ABSTRACT

Semi-stabilized dune systems are important indicators of Quaternary drought variability across central North America. The South Texas sand sheet (STSS) is the southernmost relict dune system in central North America and is exposed to higher evapotranspiration and moisture variability than similar landscapes farther north. This study uses multi-scale analysis of LiDAR data, geophysical surveys, optically stimulated luminescence dates of core samples, and X-ray fluorescence analysis to identify historical periods of desertification across the STSS. These data suggest long-term relationships between climate, ecological disturbances, geological framework, and desertification. Aeolian activations dated at ca. 75, 230, 2000, 4100, and 6600 yr bp correspond to periods of persistent regional drought, changes in sediment supply, and anthropogenic disturbances of native ecology. From these results it appears that regionalized activation in semi-stabilized dune systems is controlled primarily by climatic variations that reduce the overall moisture available for maintaining vigorous vegetation growth, while localized activation patterns depend more on stresses related to site-specific morphodynamics as well as human activity. With enhanced aridity forecast for much of central North America through the 21$^{st}$ century, understanding the specific thresholds of desertification is an important step towards building a conceptual model of desertification in semi-stabilized dune landscapes.

# ACKNOWLEDGEMENTS

I would like to thank my committee chair, Dr. Houser, and my committee members, Dr. Bishop, Dr. Everett, and Dr. Tchakerian, for their guidance and support throughout the course of this research. Additionally, I would like to thank Dr. Smeins from the Ecosystem Science and Management Department, and Dr. Ewing from the Geology Department, for providing field experiences that enabled me to work as effectively as possible at my own sites.

Thanks also go to my friends and colleagues in the Departments of Geography, Oceanography, Geology, and Ecosystem Science and Management. More specifically, thank you Phil Wernette, Sarah Trimble, Brad Weymer, and Andy Evans for making my field and laboratory work enjoyable. An enormous thank you to P.J. Hourahan for assisting in the collection and XRF analysis of soil cores. And thank you to the Coastal group – Brianna, Tess, Swann, Jackie, Mallorie and Ryan – for being wonderful colleagues.

Finally, thanks to my family for their encouragement and support. This dissertation wasn't written in an office, or in a vacuum. It was written in four states, three time zones, and two hemispheres. In airplanes, libraries, cafes, parks, hospitals, and bars. None of it would have been possible without my colleagues, friends, and family.

## CONTRIBUTORS AND FUNDING SOURCES

This work was supported by a dissertation committee consisting of Professor Chris Houser (advisor), Professor Michael Bishop of the Department of Geography, Professor Vatche Tchakerian of the Department of Geography, and Professor Mark Everett of the Department of Geology.

The analyses depicted in Manuscript I were conducted in part by Iliyana Dobreva of the Department of Geography. All other work conducted for the dissertation was completed by the student independently.

Graduate study was supported by a scholarship from the College of Geosciences at Texas A&M University and a dissertation research grant from the Association of American Geographers.

TABLE OF CONTENTS

Page

LIST OF FIGURES

# 1. INTRODUCTION

Scattered across the Great Plains are hundreds of stabilized and semi-stabilized dune fields as a result of complex Quaternary patterns of drought and desertification (Loope and Swinehart, 2000; Mason et al., 2004; Cordova et al., 2005; Forman et al., 2005; Hugenholtz and Wolfe, 2005a; Lepper and Scott, 2005; Halfen and Johnson, 2014; Houser et al., 2015; Barrineau et al., 2016). Areas that are today difficult to envision as sandy desert have been repeatedly exposed to severe drought and dominated by dune landscapes, and cities like Denver, Lubbock, and Saskatoon are built upon mantles of aeolian sediment that are sensitive to desertification during arid periods and that are vulnerable to aridity that is forecast for the 21$^{st}$ century (see Fig. 19; Clark et al., 2002; Cook et al., 2004; Hugenholtz et al., 2012; Halfen and Johnson, 2013). Much of this variability is inherited from drought through the Holocene that led to widespread reactivation of aeolian sediments across the region, with localized variations in timing caused by different response and relaxation times associated with vegetation communities (Hugenholtz and Wolfe, 2005b; Baas and Nield, 2010; Hugenholtz et al., 2012; Halfen and Johnson, 2013). Because wind speeds are frequently above the threshold for transport of sand grains in these areas, degradation of vegetation communities can lead to the activation of relict dune systems and rapid soil loss (Fryberger and Dean, 1979; Forman et al., 2009). Once reactivated, these systems retain vulnerability to prolonged desertification because of stored aeolian sediments and relatively sparse vegetation cover, and tend to follow

nonlinear trajectories between arid and humid steady states (see Hugenholtz and Wolfe, 2005a, 2005b)

Understanding thresholds in desertification across the Great Plains is paramount to accurately predicting how the region will respond to anthropogenic climate change in the 21st century. A number of researchers have investigated Holocene and Pleistocene histories of dune activation across the Great Plains use a mixture of dendrochronology, palynology, dune morphometry and stratigraphy, and fluvial entrenchment as proxies for regional drought (see Halfen and Lancaster, 2016 for a comprehensive listing). Specific rates of desertification and dune stabilization, and the relative influence of individual parameters on these processes, can vary greatly between dune systems and within a single system (see Wolfe and Nickling, 1993; Hugenholtz and Wolfe, 2005b; Baas and Nield, 2010). There have been periodic drought events across the Great Plains with a remarkable level of spatial and temporal synchronicity through the Holocene (see Halfen and Johnson, 2013; Halfen and Lancaster, 2016). Across the Central and Southern Great Plains, these include events at ca. 6000, 2000-4000, and 1000 yr bp (Halfen and Lancaster, 2016). With enhanced drying predicted for much of central North America, and extensive groundwater depletion precluding the option of using aquifers to balance the surface water budget studies of environmental histories in previous desert landscapes will be crucial to helping researchers understand landscape evolution and inform responsible environmental planning (Kustu et al., 2010; Hugenholtz et al. 2012; Halfen and Johnson, 2013; Brena-Naranjo et al., 2014).

Near the southernmost extension of the Great Plains lies the South Texas Sand Sheet (STSS), a semi-stabilized dune sheet with a diverse array of soils, vegetation communities, and aeolian sands of Holocene age overlying Quaternary and Pleistocene alluvium (Forman et al., 2009). Activations in the STSS discussed herein are correlated with the previous chronology published from the study region (Forman et al., 2009) and are associated with widespread regional drought across the Southern High Plains in New Mexico, Texas, and Oklahoma (Holliday, 1997; Frederick, 1998; Grissino-Mayer, 1996; Hall and Penner, 2012). In this respect, it is quite similar to many of the relict dune systems farther north. However, there are two important distinctive qualities of the STSS that make it valuable to scientific investigation. First, as it is the southernmost extension of Great Plains dune systems drought vulnerability across the STSS is enhanced significantly compared to dune systems farther north, because it is exposed to higher evapotranspiration rates than any other similar relict aeolian landscape (Norwine et al., 1978; LeHouerou and Norwine, 1987; Norwine and Bingham, 1987; Yu et al., 2006). Second, the STSS and surrounding areas were inhabited as early as the 17$^{th}$ century and explored by Spanish and Mexican settlers who kept detailed notes on the ecology and morphology of the region. As a result, there are historical records of various system states that may be qualitatively compared to modern conditions. These include the 19$^{th}$ century diaries of General Manuel de Mier y Terán, botanist Jean Louis Berlandier, and local accounts of ecological changes (see O'Shea, 1935; Berlandier, 1980; Jackson, 2000). These documents collectively suggest a gradual increase in the coverage of woody shrubland vegetation types over the previously dominant tallgrass prairie since the early 19$^{th}$ Century.

This study uses a mixture of sedimentological, geophysical, geochemical, and topographical information to build upon the existing conceptual framework of the Holocene history of the STSS. Historical accounts from colonial era explorations and reports corroborate climate reconstructions, and offer qualitative descriptions for how the landscape would have appeared before European influence. Soil core locations were selected according to geospatial and geophysical analyses designed to determine sites that maximize potential historical information (see Houser et al., 2015; Barrineau et al., 2016). Based on the results of this study, there are desertification periods associated with precipitation thresholds via Palmer Drought Severity Indices ('PDSI'; Palmer, 1968; Alley, 1984; Forman et al., 2001; Cook and Krusic, 2004), ecological thresholds observed through historic reports (O'Shea, 1935; Fulbright et al., 1993), and sediment availability in a transport-limited environment (see Brown et al., 1977).

# 2. DECONSTRUCTING AEOLIAN LANDSCAPES

## Background

Across the Great Plains of the United States and Canada there are a number of relict dune systems associated with climate changes over the Quaternary (e.g. Loope and Swinehart, 2000; Mason et al., 2004; Cordova et al., 2005; Hugenholtz and Wolfe, 2005a; Lepper and Scott, 2005; Houser et al., 2015; Barrineau et al., 2016). These systems have an abundance of sediment available for transport, are frequently subjected to winds exceeding threshold velocities for aeolian transport, and during humid periods are stabilized by dense vegetation communities dominated by tallgrass prairie and dense shrub thickets (Forman et al., 2009; Halfen and Johnson, 2013).

Extended and sequential drought causes a gradual thinning of vegetation and relict dune patches coalesce into larger continuous systems and induce more widespread desertification (Hugenholtz and Wolfe, 2005a; Hugenholtz and Wolfe, 2005b). As a result, antecedent patterns of aeolian activation result in complex morphometries affecting surface evolution by creating localized patches of relict dunes alongside older weathered aeolian deposits (Thomas and Wiggs, 2008; Telfer et al., 2010; Halfen and Johnson, 2013). There is a delayed, nonlinear response of these systems to climate change, in which active systems may persist through humid periods and stabilized dunes may remain in place during enhanced aridity (Hugenholtz and Wolfe, 2005a; Hugenholtz and Wolfe, 2005b). Piecing together localized histories of activation and stabilization is crucial for understanding how these systems have evolved in response to changes in the climate

through the Holocene (e.g., Woodhouse and Overpeck, 1998; Hugenholtz and Wolfe 2005a; Sridhar et al., 2006; Miao et al., 2007; Mason et al., 2009), and how they may react to future changes in climate (Muhs and Holliday, 1995; Thomas et al., 2005; Thomas and Wiggs, 2008; Thorpe et al., 2008; Ashkenazy et al., 2012; Bhattachan et al., 2014).

Previous research on these systems relies on field-collected samples from environments representing characteristic sub-systems of an aeolian landscape like dune ridges, interdune areas, and ephemeral wetlands in dune slacks (Holliday, 1989; Muhs and Maat, 1993; Hugenholtz and Wolfe 2005b; Forman et al., 2009; Telfer et al., 2010; Halfen and Johnson, 2013). Sampling schemes are typically based on a combination of surface conditions characteristic of extended aeolian activity (see Halfen and Johnsons, 2013), or previous studies delineating recent aeolian deposits versus older phases of dune activity or a lack of aeolian activity (see Forman et al., 2001; Hugenholtz et al., 2012; Halfen and Johnson, 2013; Holliday, 2014). As a result, areas with characteristically aeolian landform remnants tend to receive more attention in surveys, introducing a level of selection bias in sampling schemes that leads to researchers overlooking more subtle aeolian morphometries indicative of older, more weathered dune phases. In the previous published chronology of dune activity in South Texas, dated samples were collected from two sites identified as relict parabolic dunes based on morphometry and identified aeolian activity at ca. 100 yr bp, 200 yr bp, 2000 yr bp, and 2700 yr bp (Forman et al., 2009). These periods are associated with regional-scale drought and imply a climate control on dune activation, but are unable to clarify localized dynamics influencing desertification.

Barrineau et al. (2016) presented a method for guiding field-based sampling using multi-resolution analysis of LiDAR data to identify distinct phases of dune activity based upon morphometries in a small portion (roughly 25 $km^2$) of the central South Texas sand sheet. This study expands on the methodology presented in Barrineau et al. (2016) by extending the study area to 3000 $km^2$ and comparing results to geochemical and grain size analysis of field-collected soil cores to investigate the efficacy of this method. High-resolution elevation models are processed using multi-resolution analysis and Principal Components Analysis (PCA) that discretizes topographic variations indicating different phases of aeolian activity across the sand sheet. This method is designed to enhance field-based sampling by avoiding selection bias, and therefore enhances the validity of system-wide conclusions from a handful of soil cores. By producing a comprehensible, discrete visualization of distinct process-form regimes, this study directly addresses difficulties associated with geomorphological mapping as described in Bishop et al. (2012).

Study Site

The South Texas Sand Sheet (STSS) dominates the Gulf Coastal Plain between Corpus Christi and the Rio Grande and has undergone multiple phases of dune activity throughout the Holocene associated with climate and anthropogenic influence (Fig. 1; Griffith et al., 2004; Forman et al., 2009). The STSS lies across over 7000 $km^2$, and the sandy substrate alters vegetation communities such that localized histories of dune activation remain influential in landscape evolution for several generations of succession (Fulbright et al., 1990; Smeins et al., 1991). A steep gradient between sub-humid and semi-arid climates (annual rainfall decreases from over 800 mm to less than 600 mm across the system)

means that the STSS is particularly susceptible to changes in regional circulation causing enhanced drought (Johnston, 1963; Diamond and Fulbright, 1990). Moreover, as the southernmost extension of Great Plains dune systems, the STSS is subject to relatively high evapotranspiration rates so that even during a wet year, the balance of moisture retained remains below similar landscapes further north (Yu et al., 2006). This moisture gradient and enhanced susceptibility to drought makes the STSS an ideal natural laboratory for examining histories of aeolian activity.

Topographic variation in the STSS is greater in younger dune patches, while older dune forms retain little or no surface roughness. The primary lasting effect of older dunes occurs via pedogenesis – stabilized aeolian sands allow rapid infiltration and retain relatively low organic content. Vegetation assemblages across the STSS reflect its diachronous activation history through concomitant differences in soils and vegetation communities (Fulbright et al., 1990). The dominant communities are tallgrass prairie with some horizonation (inceptisols), sparse sandy grasslands with little horizonation (entisols), and patches of dense woody vegetation known as 'mottes' with developed soils (alfisols). This diverse mosaic of ground covers alters surface roughness, but active dunes often migrate over otherwise healthy and functioning grasslands and woodlands. Dead stands of live oak (*Quercus virginiana*) and honey mesquite (*Prosopois glandulosa*) remain in interdune areas as a testament to the inability of woody vegetation to fully stop dune advance, and are a common phenomenon across the STSS (Fig. 2).

A mixture of Entisols, Inceptisols, and Alfisols dominates the soil orders found across the study area. These are associated with the Cayo, Topo, Falfurrias, Nueces and Sarita

series, respectively, and the variability is related to distinct aeolian process-form regimes like relict dune ridges, interdune areas, and hummocky deflation plains. The Falfurrias soils are located in very young dune forms that have undergone minimal stabilization and horizonation, while the Nueces and Sarita soils are located in areas with much older, massive aeolian sands displaying more distinct horizons and mature vegetation communities. The Cayo and Topo soils display some horizonation but occur in areas with characteristically aeolian topography, suggesting they are an intermediate age somewhere between the older Alfisols (Nueces and Sarita series) and the younger Inceptisols (Falfurrias series).

In other aeolian landscapes across the Great Plains, variations in surface material and vegetation assemblages reflect divergent activation chronologies (Loope and Swinehart, 2000). Dune activations in the STSS correspond to ca. 100 and 200 yr bp, when enhanced aridity during the mid 20$^{th}$ century (PDSI -4.3) and 1789-1790 AD (PDSI -3.8 and -4.7) and the introduction of livestock during the 18$^{th}$ century promoted the growth of shrublands (O'Shea, 1935). Activations at ca. 2000 and 2700 yr bp are contemporaneous with regional drought on the Southern High Plains (Fulbright et al., 1990; Forman et al., 2009). These results suggest a regional climate control on desertification patterns, but also imply localized activations could be affected by anthropogenic influences like agriculture. Decomposing the spatial variance of aeolian deposits across the STSS using morphometry as a proxy for divergent process-form relationships represents a useful approach for identifying antecedent conditions that continue to influence patterns of dune activity.

Methodology

**LiDAR Data**

The LiDAR data were collected in 2009 as part of the National Elevation Dataset (NED) program. A digital elevation model was derived from raw point clouds at a spatial resolution of 3 $m^2$ for our study area, which covers roughly half of the sand sheet. Multi-resolution analysis was used to generate 21 DEMs from the original elevation model representing different spatial resolutions. A Gaussian filter was used to calculate average altitudes at each pixel using intervals designed to capture scale-dependent topographic variation across the study area resulting from different phases of aeolian activity. A 5 m interval was used out to a distance of 30 m, and a 30 m interval was used from 30 to 480 m for each grid cell location. The larger interval was used to measure differences in morphology at a larger scale, while the smaller interval was used to identify changes within individual dunes. Each successive Gaussian filter progressively represents more generalization with respect to the true elevation value (e.g., Filter 1 = 5 m, Filter 2 = 10 m…Filter 6 = 30 m, Filter 7 = 60 m…Filter 22 = 480 m). This way variations that influence wind flow and the migration patterns of active dunes are weighted as much as variations reflecting past activations and more weathered large-scale dune forms.

**Principal Components Analysis**

PCA is commonly used to reduce large data sets based upon the degree of multicollinearity, such that it isolates or extracts the significant linear variance components from the dataset (Jensen, 2005). PCA has been used with satellite imagery (Fung and LeDrew, 1987; Rodarmel and Shan, 2002) and RADAR (Grunsky, 2002; Guitet

et al, 2013) to assess variations in vegetative cover and mineralogy, to analyze topographic variations characteristic of distinct process-form regimes (Wright et al., 1985; Plant and Griggs, 1992; Kuriyama and Lee, 2001; Houser et al., 2008; Houser and Hamilton, 2010), and with seismic data to identify distinct strata (Guo et al., 2009; Coleou et al., 2003). However, geomorphological studies using PCA for analyzing multi-resolution datasets are rare, as multi-resolution data are not routinely generated, and software may not be readily available. By improving upon previous multi-resolution analyses from this landscape (Barrineau et al., 2016) and comparing the PCA output to field-collected soil cores, this study offers a more robust assessment of this methodology in semi-stabilized aeolian environments.

Barrineau et al. (2016) used PCA based on a similar multi-resolution dataset across a smaller portion of the South Texas sand sheet, and found that topographic variation could be used to identify relict aeolian landforms not evident in the original DEM or imagery. Their multi-resolution analysis calculated average elevations at 20 m intervals out to 1000 m, and as a result lent more attention to large-scale dune forms (e.g. length scales of >200 m, larger than most active dune patches). Their interpretation of the final PCA output was able to identify differences between aeolian morphometries, but was somewhat hampered by an overwhelming statistical dominance of the first component, which was loaded heavily in active and recently stabilized dune systems. They concluded that variations in less heavily loaded components (e.g. Components 2, 3, and 4) revealed valuable morphometric information indicating distinct process-form regimes like zones of aeolian deposition and deflation. In this study, the PCA input (e.g. multi-resolution data set) is

designed to specifically capture smaller-scale variations in elevation along with these large-scale morphometries. Length scales associated with localized variations in topography amongst active and recently stabilized dune systems are identified by 5 m intervals, while 30 – m intervals are scaled in order to characterize larger-scale variations associated with heavily weathered relict aeolian landforms covered in vegetation.

The multi-resolution dataset was analyzed using unstandardized PCA based upon the covariance matrix, and produced a series eigenvalues and eigenvectors. Eigenvalues describe the variance structure of each component with respect to the total variance of the multi-resolution dataset (i.e., how much variance each component represents). Eigenvectors represent the coefficients that are used to transform the multi-resolution dataset into components, and they describe the contribution of variance from a particular portion of the data set to each component (in this case, at particular spatial scales). After generating the components, an unsupervised k-means algorithm was used to generate a classification that provides a more discrete visualization of distinct morphometries.

**Field-Collected Cores**

Six soil cores were collected in order to test the veracity of our hypothesis that the PCA output is in fact identifying distinct aeolian morphometries. Using the results of Barrineau et al. (2016) and soil surveys of the Natural Resource Conservation Service (NRCS) to select sampling sites arranged to capture multiple distinct environments of the STSS, cores were collected during the summer of 2015. The locations of these samples were chosen specifically to maximize the amount of historical information on aeolian activation by sampling within a mixture of subdued and more recent aeolian

morphometries. Cores 1&2 were collected along a topographic gradient, placed specifically to test the ability of multi-resolution PCA to discretize small-scale changes in morphometry indicating distinct process-form regimes (Focus Area 1). Cores 3&4 were collected away from active or recently active dunes, but at locations that the PCA output identified as being characteristically aeolian (Focus Area 2). Cores 5&6 were collected in areas with hummocky topography and relatively young prairie vegetation communities (Focus Area 3).

The collected cores range in depth from 90 cm to 150 cm, and were collected manually using PVC pipe housing. XRF analysis was performed on split cores in the Integrated Ocean Discovery Program (IODP) laboratory at Texas A&M University using a third-generation Avaatech XRF Core Scanner. Cores were split, separated, and sampled at 1 cm intervals. Excitation was performed at 10 and 30 kV, and measured elemental intensities for major elements between Al and U. Grain size measurements were collected in the laboratory using a Horiba Camsizer (www.horiba.com), which digitally images and analyzes thousands of particles for each sample. Samples were collected from split cores at 10 cm intervals and run through the camsizer for 5 minutes each. Detection limits for the camsizer were selected from Wentworth scale grain sizes, ranging from 0.063 – 0.5 mm, and distributions were collected at $10^{th}$, $50^{th}$, and $90^{th}$ percentiles.

Results

Final PCA output reveals that 99.9% of the topographic variation in the multi-resolution dataset is contained in the first four components. Thus, we have focused on these four components in our discussion. Component 1 contains the most variance (98.8%)

and has the strongest eigenvector loadings with spatial scales <200 m, close to the length scale of active dune patches in the study area. The areas highlighted spatially by Component 1 are active and recently active dune patches, as evidenced by contemporary (2015) and historical (1952) NAIP imagery (NETR, 2015).

Components 2, 3, and 4 offer more detailed information regarding specific process-form regimes at the surface (Fig. 2). Component 2 highlights areas dominated by recent aeolian deposition such as dune crests and lee slopes (see Fig. 3, top left). Component 3 highlights areas dominated by recent aeolian erosion such as deflational flats upwind of active dune patches. Component 4 (see Fig. 3, middle left) highlights relict aeolian forms such as precipitation ridges left by migrating dune patches (see Fig. 3, bottom left). Based on the field-observed relationships between these three components and distinct aeolian morphometries, we created a clearer, discrete output through a layer stack and classification. When compared to satellite imagery and elevation models of the study area (Fig. 1), the classification of Components 2, 3, and 4 highlights areas of topographic variation that are not visibly apparent in digital elevation models and possibly represent older aeolian landforms. A qualitative comparison of this output to soil surveys shows that there is a spatial relationship between major soil orders and patterns in the classification output (see Fig. 4). Specifically there are three distinct zones across the study region: areas with hummocky topography and undeveloped soils, areas with little topographic variation and more developed soils, and areas without hummocky topography and more developed soils.

Three focus areas were identified as representative environments of the three regimes and two soil cores were collected from each. The first (Focus Area 1, Cores 1&2, Fig. 5, Fig. 6) is located along a sharp gradient in surface roughness associated with the border between hummocky and low relief topography. Moreover changes in soil series and regimes associated with morphological differences show similar spatial variations to those seen in the PCA classification (see Fig. 4). Core 1 is situated near a dense patch of woody vegetation, while Core 2 is located in tallgrass prairie with more topographic variation. The second (Focus Area 2, Cores 3&4, Fig. 7, Fig. 8) is located in an area with little topographic variation, but that the PCA classification (and soil surveys) suggests is characteristically aeolian. Core 3 is situated adjacent to an active dune patch, within an area identified through the classification as characteristically aeolian. Core 4 is situated away from any active or relict dune features, in an area covered with massive sands that have not experienced erosion or deposition for quite some time. The third (Focus Area 3, Cores 5&6, Fig. 9, Fig. 10) is located within undulating hummocky topography surrounded by active dunes, and is presumably the portion of the study area that has undergone aeolian activation most recently. Core 5 is located upwind of an actively migrating dune patch on a deflation plain surrounded by trailing ridges and remnant knobs. Core 6 is situated among hummocky topography with active dune patches in all directions.

XRF analysis suggests Core 1 is part of the Topo series inceptisol, occurring in aeolian soils with virtually no topography, and Core 2 is a Falfurrias entisol, occurring in stabilized sand dunes of South Texas with slopes ranging from 0 to 15% (NRCS, 2016). The cores' geochemical profiles show differences in horizonation and grain size confirming this

classification. A mixture of inverse Si and Ca concentrations, along with accumulation of Fe around 80 cm depth dominates Core 1 while Si overwhelmingly dominates Core 2 with variations in concentration representing historical aeolian depositions (Fig. 6). The distinct horizonation in Core 1 suggests it is part of the Topo series, while the subdued horizonation in Core 2 suggests it is part of the Falfurrias series.

XRF analysis suggests Core 3 is a Nueces series alfisol, occurring in deep aeolian soils of South Texas overlying older Quaternary alluvium (NRCS, 2016). XRF analysis suggests Core 4 is part of the Sarita series alfisol, which is similar in provenance to the Nueces but features more distinct horizonation (NRCS, 2016). Si overwhelmingly dominates Core 5 with variations implying multiple phases of aeolian deposition, while Core 10 shows enhanced soil development via eluviation around 1 m depth (Fig. 8).

XRF analysis suggests Cores 5 and 6 are part of the Falfurrias series entisol, occurring in stabilized sand dunes of South Texas with slopes ranging from 0 to 15% (NRCS, 2016). There is a spike in elemental intensities associated with a perched water table in Core 6, but beyond this the geochemical profiles cores show little horizonation, suggesting this classification is correct. Si overwhelmingly dominates both cores with slight variations in concentration likely representing historical aeolian depositions (Fig. 10). Historical imagery of both sites shows they were covered in migrating aeolian sands within the past century, further suggesting these are derived from a recent activation period (see Fig. 11).

Discussion

The associated differences in horizonation shown through XRF analysis and published soil surveys, paired with the classified differences in morphometry shown in the PCA

results, suggest scale-dependent topographic variations are associated with not only process regimes but also historical patterns of dune activity. Based upon previously published chronologies of the system and varying rates of soil development (used as a proxy for time elapsed since stabilization), this classification is revealing relict dune forms that are not prominent in elevation models and imagery, and are nearly impossible to identify in the field. As a result these landforms are easy to miss, and would likely be overlooked by researchers planning field investigations designed to assemble a landscape history.

Component 1 represents 98.8% of the statistical variation across the dataset. It largely highlights recently active dune forms and offers little information about specific process-form regimes within and between active and relict dune patches. The statistical weight of small-scale elevation variations (like those found in active aeolian bedforms) is a parameterization of the fact that hummocky topography dominates much of the study area. The use of 5 m intervals in calculating the multi-resolution dataset means that this Component's statistical dominance is reflecting the spatial dominance of small-scale roughness features like individual dunes and remnant knobs across the landscape. Components 2, 3, and 4 tend to favor areas with more recent aeolian activity as well, but offer important distinctions between the types of topographic variation observed across the study area that we believe are useful for delineating aeolian deposits of distinct phases.

In Focus Area 1, there is a sharp gradient in topographic roughness dividing recent dune forms made of inceptisols to the southwest and older aeolian entisols to the northeast. This gradient is evident in the PCA output but is much less clear in visible imagery and

the original elevation model (Fig. 5). The PCA classification identifies this gradient and correctly identifies areas with enhanced surface roughness as aeolian. In the low relief areas, the classification identifies a number of locations that when viewed collectively retain the characteristic shape of parabolic dunes with narrow trailing ridges (Fig. 5). This suggests that this gradient represents a process-form regime shift between younger and older aeolian deposits. Based on the XRF results, both core sites are located within areas of distinct aeolian morphometries identified by the PCA results (Fig. 6). Based on the horizonation evidenced by the cores, the Topo series (Core 2) is inherited from a much older phase of dune activity, confirming the PCA classification's results showing these two cores as members of distinct process-form regimes within the younger and intermediate – age aeolian morphometries of the STSS.

In Focus Area 2, there is an actively migrating dune system in the south-central portion and topographically featureless flats hosting a complex mosaic of woody vegetation dominated by alfisols. Within the low-relief areas, the PCA classification identifies subtle variations in topography as characteristically aeolian. Core 3 is located within a large relict parabolic arch, according to the PCA results, but is dominated by deep, massive aeolian sands without morphometric evidence of recent dune activity (Fig. 7). Core 4 is located several hundred meters away from the nearest apparent dune form that could be identified in the field but is identified in the PCA as characteristically aeolian, suggesting it may be within a much older dune phase. The enhanced horizonation and lack of proximity to other areas featuring evidence of dune activity in and around Core 4 suggests it was stabilized before Core 3, which shows little horizonation besides Si variation (Fig. 8). Based on these

observations, and the PCA results classifying Core 3 within an aeolian landform, the Nueces soils could be derived from a relatively younger dune phase. The geochemical profiles and PCA results suggest the Sarita series is part of a dune phase older than the Nueces to the point that most topography and horizonation-based evidence has been effaced into the modern surface.

In Focus Area 3, there is extensive hummocky topography covered in prairie grasses with no wooded vegetation. The PCA classification identifies several areas within a few hundred meters of the coring sites as being characteristically aeolian, and there are actively migrating dunes in every direction (Fig. 9). Core 5 is located within a large deflation plain bordered by trailing ridges and scattered with remnant knobs. Core 6 is surrounded by small deflation flats and located along a continuous series of remnant trailing ridges. In both cores there is little horizonation besides Si variations (Fig. 10). The lack of horizonation, along with historical imagery showing these areas were covered with migrating dunes within the past half century (see Fig. 11), suggests these cores are part of the Falfurrias Entisol that represents the most recent phase of aeolian activity in the STSS.

Collectively, these geochemical and morphometric results suggest there are at least three phases, and possibly four phases, of dune activity in the STSS. The youngest phase of activity is expressed at the surface by the Falfurrias series with a high degree of topographic variation. Based upon historical imagery (1952), most of these areas were active within the past century and are most likely inherited from 20$^{th}$ century aridity, or anthropogenic disturbances caused by the growth of ranching over the past two centuries. The Topo series commonly occurs in relict interdune areas that are frequently flooded and

feature more horizonation than the Falfurrias series, and is most likely inherited from the penultimate dune phase occurring around 18$^{th}$ century droughts as evidenced in regional climate records and previous studies of the STSS (Yu et al., 2006; Forman et al., 2009). Finally, the Sarita and Nueces series express the oldest dune phases at the surface. According to the NRCS soil surveys, these series are alfisols dominated by deep aeolian sands and more horizonation than what is found in the Topo and Falfurrias inceptisols and entisols. The Nueces series occurs on "vegetated low dunes" that the PCA successfully identified, and are probably from the 2000 yr bp activation phase. The Sarita series is associated with morphometric evidence of aeolian activity based upon the PCA results and more horizonation, and is most likely inherited from an older period of dune activity not yet identified in the published literature.

The results presented herein show that the multi resolution PCA analysis is able to identify distinct multi-scale topographic variations associated with aeolian landforms of different ages. Field collected soil samples confirm the PCA-based classifications identifying relict dune landforms. These findings suggest the multi resolution PCA is a useful first step for field-based investigations of dune activity in semi-stabilized aeolian landscapes, and should be used to identify aeolian landforms that may not be immediately recognized in elevation models, visible imagery, or even field excursions.

## Conclusions

There are a range of topographic variations between distinct phases of dune activity on the South Texas Sand Sheet and other stabilized aeolian landscapes of the Great Plains. The multi-resolution analysis and PCA successfully identified distinct variations that

correspond to modern process-form regimes as well as historical patterns of dune activation and stabilization. These divergent local histories interact with hydrological and ecological dynamics to create a highly diverse mosaic of vegetation communities as well as landform assemblages. Characterizing these differences and producing a comprehensible, discrete visualization of these different systems contributes to the body of knowledge regarding the Holocene evolution of South Texas and the Great Plains. It is clear that multi-scale topographic information can be used for identifying areas of distinct modern and historical process-form regimes, and in doing so provide a context for future field investigations of the STSS. Future analyses of the field-collected cores including more extensive luminescence and/or carbon dating would enable researchers to place these distinct morphometries and soil series in discrete time periods and compare regional climate records, previously published dates, and contemporary conditions in morphometry, soils, and vegetation communities affecting the present state of the STSS.

# 3. CAN ELECTROMAGNETIC INDUCTION PROFILERS DELINEATE AEOLIAN SEDIMENTS?

## Background

There are semi-stabilized dune systems across the Great Plains of North America that have undergone repeated cycles of desertification and soil development through the Holocene (Loope and Swinehart, 2000; Mason et al., 2004; Cordova et al., 2005; Forman et al.. 2005; Hugenholtz and Wolfe, 2005a; Lepper and Scott, 2005; Forman et al., 2009). These systems are characterized by extensive near-surface sand deposits and are frequently subjected to winds higher than threshold velocities for aeolian transport, so are vulnerable to cycles of stabilization and re-activation (Hugenholtz and Wolfe, 2005b; Halfen and Johnson, 2013). A mixture of climate, ecological, and anthropogenic controls inform the stabilization and activation of these systems, and result in heterogeneous patches of migrating dunes interspersed amongst semi-stabilized wind blown sediment (Clark et al., 2002; Hugenholtz and Wolfe, 2005b).

Periods of aeolian instability are characterized by active dune migration, and occur following changes in stress on native prairie and woodlands (Madole, 1994; Clark et al., 2002; Cook et al., 2004; Hugenholtz and Wolfe, 2005b; Hugenholtz et al., 2012; Halfen and Johnson, 2013). This can be caused by drought (Dean et al., 1996; Cook et al., 2004; Forman et al., 2009), changes in sediment supply (Muhs et al., 1999), or reduction in vegetation cover from anthropogenic stress (Wolfe et al., 2007). Moreover, inherited patterns of aeolian erosion and deposition result in varying rates of sediment accumulation

and thickness across a single dune system. As a result there is often a complex underlying stratigraphy informing surface moisture supply and sediment availability.

Within semi-stabilized dune systems, different soil regimes reflect distinct aeolian process-form regimes and react to climate, ecological, and/or anthropogenic stresses in different ways. For example, relatively coarse grains would dominate high-energy migrating dunes, while relatively small grains either accumulate in ephemeral wetlands and/or are blown as dust to the downwind margin of actively migrating dune patches. As dunes stabilize, these patterns persist so that it is possible to identify the provenance and transport dynamics of grains based on their size, sorting, and geometry (see Muhs et al., 1996). Additionally, soil variations in semi-stabilized aeolian landscapes reflect predominantly the most recent activation periods so that relatively younger soil orders (i.e. inceptisols, entisols) are likely to have undergone more recent erosion and deposition than older soils (i.e. alfisols).

Previous research on Great Plains dune systems often utilized a combination of spatial analysis of imagery, elevation models, and field-collected samples analyzed using X-ray fluorescence (XRF) scans, $^{14}C$ dating, and optically stimulated luminescence (OSL) or thermoluminescence (TL) dating (Holliday, 1989; Muhs and Maat, 1993; Hugenholtz and Wolfe, 2005a; Forman et al., 2009; Telfer et al., 2010; Halfen and Johnson, 2013). Because these landscapes can be quite large (e.g. >1000 $km^2$ is not uncommon), sampling schemes are often widely dispersed with little information available between sample points. Researchers must often make conclusions based upon sparse observations, and these conclusions are difficult to justify if adjacent observations are uncorrelated. Identifying

methods that enable characterization of surface and near-surface sediments between sampling points is a crucial step in improving methodologies to investigate these landscapes. More specifically, being able to identify spatial variations in moisture content that affect vegetation communities and soil moisture is an important step to understanding the dynamics of these systems.

Electromagnetic induction (EMI) profilers measure spatial variations in electrical conductivity of the shallow subsurface. Conductivity variations are associated with variations in soil properties such as grain size, salinity, and moisture. Portable EMI profilers (commonly termed 'terrain conductivity meters') are useful tools since they offer a non-invasive method capable of covering relatively large study areas in a short amount of time, at a reduced cost compared to more traditional EMI instrumentation. EMI profiling has been used in precision agriculture to identify soil series with the goal of maximizing crop growth (Corwin and Lesch, 2005; Robinson et al., 2009; Sudduth et al., 2013), and the success of this method in delineating soils with different properties is well established (Corwin and Lesch, 2005; Triantafilis and Lesch, 2005; Sudduth et al., 2005; Triantafilis and Buchanan, 2009; Andre et al., 2011; Everett, 2012). However, relatively few studies have used EMI profiling to classify soils in semi-stabilized aeolian systems. Such systems are marked by heterogeneity in surface and subsurface material that reflect historical patterns of desertification and stabilization.

X-Ray fluorescence (XRF) core scanning is widely used for analyzing submarine as well as subaerial sediment cores to generate environmental reconstructions based upon soil provenance and age, inferred from properties such as mineralogy, grain size, and

stratigraphy (Jansen et al., 1998; Arz et al., 2001, 2003; Lamy et al., 2001; Andres et al., 2003; Weltje and Tjallingii, 2008). While there are a number of theoretical difficulties associated with XRF as a robust environmental reconstruction methodology (see Rothwell and Rack, 2006), the utility of XRF core scanners lies in their ability to deliver elemental *intensities* as raw data. While studies focused on generating mass balance and flux constraints for landscape modeling require specifically calibrated values of elemental *concentrations* to make their calculations as robust as possible, the *intensity* of various elements within a split core is useful for qualitatively identifying subsurface heterogeneities (see Haug et al., 2003, and Haschke, 2006). Because this study uses XRF analysis simply to verify existing soil surveys – as opposed to constraining mass balance or flux modeling of sedimentary dynamics – elemental intensities are sufficient, and we did not pursue more complex calibrations of measurements in order to calculate specific elemental concentrations (see Rothwell and Rack, 2006, and Weltje and Tjallingii, 2008).

This main purpose of this study is to demonstrate the utility of EMI profilers in delineating soil regimes across semi-stabilized dune systems, and to compare observed EMI data with field-collected soil samples analyzed using XRF and grain size analysis. This is done to construct a continuous high-resolution conceptual model of the structure and soils across a central portion of the South Texas sand sheet.

Study Site

The South Texas Sand Sheet (STSS) is an extension of the West Gulf Coastal Prairie (EPA Level III No. 34) that overlies an area in excess of 8000 $km^2$ between Corpus Christi and the Rio Grande (Griffith et al., 2004; Forman et al., 2009). A study area within the central STSS was selected to demonstrate the utility of EMI profilers in semi-stabilized aeolian landscapes. The study area measures roughly 50 $km^2$ and is located along a strong gradient in soils, topography, and vegetation communities. Winds are annually bimodal, with a dominant southeasterly flow during summer and a secondary northerly flow during winter (Texas Commission on Environmental Quality, 2008; see Fig. 12). Sediments across the study area are uniformly aeolian with very little internal stratification (USDA NRCS, 2016), so most of the conductivity variations measured with the EMI profiler should reflect subtle shifts in grain size associated with the various aeolian morphologies distributed across the larger landscape. These include relict and active barchanoid dunes, trailing dune ridges, remnant knobs, and small ephemeral wetlands in deflation basins on the upwind side of dunes.

Sandy surface material in the STSS alters vegetation communities and hydrological regimes from adjacent coastal tallgrass prairies much in the same way as the Nebraska Sand Hills contain ecologically distinct zones from adjacent rangelands (Archer and Smeins, 1991; Fulbright et al., 1993). There is a steep climate gradient across the study area between sub-humid and semi-arid: annual rainfall decreases from over 800 mm to less than 600 mm in a span of less than 80 km, which means the landscape is particularly

susceptible to drought compared to more humid dune systems further north (Johnston, 1963; Diamond and Fulbright, 1990).

Soils across the South Texas sand sheet are highly variable, and there are ten or more soil series comprising three major soil orders across the region (USDA NRCS, 2016). Variations in localized soil series are a combined reflection of recent dune activity and differences in vegetation succession in soils of various ages (Diamond and Fulbright, 1990; Fulbright et al., 1993). Vegetation assemblages across the STSS include tallgrass prairie, sparse sandy grasslands, shallow wetlands, and dense groves of live oak (*Quercus virginiana*) and honey mesquite (*Prosopis glandulosa*) known as 'mottes' (Fulbright et al., 1990). Under humid conditions, vegetation succession and soil development result in a complex mosaic of groundcovers (Diamond and Fulbright, 1990; Archer and Smeins, 1991; Fulbright et al., 1993). This generates surface roughness and creates heterogeneous patterns of patchy migrating dunes interspersed with thriving grasslands and mottes. The persistence of aeolian sands or clay lenses in the subsurface influences the groundwater hydrology and can affect vegetation development (Diamond and Fulbright, 1990; Fulbright et al., 1993).

In the only published sedimentological analysis from the STSS, epochs of historic dune activity have been dated at roughly 100 yr bp, 200 yr bp, 2000 yr bp, and 2700 yr bp (Forman et al., 2009). The most recent dated activation is probably climate-driven and related to a series of droughts in the first half of the twentieth century, while the penultimate activation may correspond to a 1789-1790 AD drought in which the Palmer Drought Severity Index (PDSI) of the study area was -3.8 and -4.7, respectively (Cook

and Krusic, 2004; Yu et al., 2006; Forman et al., 2009). Early settlement of the region and the introduction of livestock may have also influenced the activation of dune systems during the 18th century, though this is difficult to confirm (Johnston, 1963; Fulbright et al., 1993; Forman et al., 2009). The 2000 yr bp and 2700 yr bp events are contemporaneous with drought in the Southern High Plains of Texas and New Mexico as well as South Texas, which suggests a regional climatic control on large-scale dune activation (Cook et al., 2004; Yu et al., 2006; Miao et al., 2007; Forman et al., 2009).

Methodology

**EMI Profiler Surveys**

Traditional EMI sensors consist of separate transmitter (TX) and receiver (RX) coils connected by cables, placed at a specific distance apart (termed the TX-RX offset). The offset is important because, along with the operating frequency, it helps to determine the depth at which the conductivity of the subsurface is probed. Variable-offset EMI profilers, such as the Geonics EM34, measure electromagnetic properties at a single frequency, with the depth of measurements controlled by varying the offset. With newer portable EMI profilers such as GSSI EMP 400, the offset is fixed by physically connecting the TX and RX coils into a single lightweight instrument that may be carried by a single individual. These profilers collect data at multiple frequencies and hence probe the surface at different depths. Higher frequencies result in greater subsurface attenuation, so there is an inverse relationship between frequency and depth of measurement. EMI data are often interpreted via spatial analysis of responses at a single frequency (Huang and Won, 2000). Because the EMI profiler we use is capable of measuring multiple frequencies simultaneously, we

focus on apparent conductivity at three frequencies, each of which probes a slightly different depth range.

This study uses a GSSI Profiler EMP 400$^{TM}$ that measures apparent conductivity at multiple frequencies ranging from 1 – 16 kHz, with 1 kHz increment, and at fixed offset 1.21 m (GSSI, 2007; Huang et al., 2008). The profiler is controlled by commands sent via a wireless Bluetooth$^{TM}$ interface that is incorporated into a TDS RECON-400 Personal Digital Assistant (PDA). GPS coordinates are recorded at each measurement location with a positional accuracy of ~1 m. In order to prevent data issues from sensor calibration at different points (see Abdu et al., 2007; Andre et al., 2011), the instrument settings remained constant through the field surveys.

Surveys were conducted during Fall 2014 at 3, 5, and 15 kHz, frequencies selected to measure conductivity within 3 m of the surface, the published depth of sand sheet deposits across the STSS (Forman et al., 2009). These data were collected at 10 m station intervals along a series of 6 transects spaced 50 m apart, with a seventh transect connecting all others (Fig. 13). The lower frequencies were specifically selected to probe beneath a nonconformity at the study site, which previous research suggests occurs at roughly 3 m beneath the surface (Diamond and Fulbright, 1990; Fulbright et al., 1993; Forman et al., 2009).

In order to visualize continuous changes in apparent conductivity across the study area, the data were interpolated between sampling points using a k-means algorithm. Limited data processing was employed on the data presented herein; apparent conductivity values are reported as observed in situ, and a 1-dimensional inversion algorithm was used to

calculate layer thickness at each sampling point in order to estimate the thickness of aeolian sediments at the surface (see Everett, 2012).

**XRF and Grain Size Analysis**

In order to associate the EMI-measured apparent conductivities with in situ variations of grain size and different soil series, two soil cores were extracted within the small study area. These cores are a subset of a larger suite of ten cores (Fig. 14). Using the results of Barrineau et al. (2016) and Natural Resource Conservation Service (NRCS) soil surveys to select sampling sites, the cores were collected during the summer of 2015. The locations of the ten cores were chosen to maximize the amount of contextual information on aeolian soils by sampling within a mixture of gentle and rugged terrain. Cores 5 and 6, used here, were placed on opposing margins of an actively migrating dune patch in the central STSS.

XRF core scanning is a useful technique to investigate geochemical properties of soil samples measured as a depth profile along a soil column. Samples are exposed to X-radiation that causes electrons to be ejected from inner atomic shells, and as electrons from the outer shells fill these vacancies they emit a pulse of X-radiation (Jenkins and DeVries, 1970). The energy and wavelength spectra of this emission, which vary based upon the element, are measured. The spectrum provides an estimation of elemental concentrations. XRF analysis requires samples to be prepared as homogeneous and smooth as possible before laboratory testing. Because split cores will always contain some variations in grain size, moisture, and shape, the conditions on sample preparation are incompatible with the reality of analyzing field-collected core samples. Moreover, the results will always be affected by the space between the scanner and core because X-radiation excited by the

XRF system will compromise the measurement of many light elements (see Rothwell and Rack, 2006). Despite these weaknesses, XRF is widely regarded as a useful technique for measuring soil properties, as a function of historical changes in biogeochemical parameters (Andres et al., 2003; Haug et al., 2003; Rothwell and Rack, 2006; Darrénougué et al., 2009).

XRF analysis was performed on the split cores in the Integrated Ocean Discovery Program laboratory at Texas A&M University using a third-generation Avaatech XRF Core Scanner. Cores were split, separated, and sampled at 1 cm intervals. Excitation was performed at 10 and 30 kV, and elemental intensities were measured for the major elements between Al and U. The output data were not subsequently calibrated to derive elemental concentrations. Because this study uses XRF analysis simply to qualitatively assess the local accuracy of soil surveys, and identify specific soil series across the study area, the elemental intensities are sufficient (see Rothwell and Rack, 2006, and Weltje and Tjallingii, 2008).

Grain size measurements were collected in the laboratory using a Horiba Camsizer (www.horiba.com), which digitally images and analyzes the sizes of thousands of particles for each sample. Samples were collected from split cores at 10 cm intervals and run through the camsizer for 5 minutes each. Detection limits for the camsizer were selected from Wentworth scale grain sizes, ranging from 0.063 – 0.5 mm, and distributions were collected at $10^{th}$, $50^{th}$, and $90^{th}$ percentiles. Average grain sphericity was also collected across all grain sizes for each sample point.

Results

EMI surveys show apparent conductivity measurements at all three frequencies ranging from 0 to 60 mS/m across the study area. Estimated thickness of the surficial sands, calculated using a 1-D inversion, range from < 1.0 m to 31.6 m. The apparent conductivities are consistent with previous research showing these conductivities to be consistent with sand (and perhaps silt) sized grains (Grisso et al., 2009; Barbosa and Overstreet, 2011). In general, conductivity increases with depth across the study area from 13.4 mS/m to 19.8 mS/m and is more uniform at the surface. The estimated thickness of the aeolian deposits at the surface suggests the STSS could be much deeper in localities than thought (Fulbright et al., 1993; Forman et al., 2009), and a more in-depth analysis of the spatial variability of this layer's thickness could contain a wealth of information on localized desertification thresholds.

Conductivities measured by the 15 kHz signal (Fig. 15) average around 10 mS/m and represent the uppermost mantle of Holocene aeolian sands deposited across the sand sheet in its most recent activation during the last century (see Forman et al., 2009). These sands lack internal stratification (massive), are generally fine to medium grained sands with little variations in grain size, and are dominated by quartz grains (Forman et al., 2009). The greatest degree of spatial variability in apparent conductivity at the surface is found within two areas that are frequently inundated by surface runoff. In these two areas, the variable conductivity is probably not influenced more by this runoff than significant changes in grain size or soil series (Dieterle and Vera, pers. comm., 2015).

Apparent conductivity values measured using the 5 kHz signal shows an average of 17 mS/m and varies spatially with topography. Areas such as windward dune slopes, stabilized trailing ridges, or deflation flats are strongly spatially correlated to variations in apparent conductivity at this frequency (Fig. 16). Conductivities measured via the 3 kHz signal (Fig. 17) average around 18 mS/m and display more spatial heterogeneity and localized patches of distinct apparent conductivities than those detected with higher-frequency EMI.

XRF results suggest that cores extracted from opposing margins of the study area (Fig. 14) conform to published soil surveys. The southeastern core (Core 6) samples the Portrero entisol, while the northwestern core (Core 5) samples the Nueces alfisol. Grain sizes observed in Core 6 are consistently fine sands, while Core 5 features very fine sands within 20 cm of the surface. Core 5 displays more enhanced horizonation than Core 6, although a perched water table at roughly 70 cm depth in Core 6 is associated with a spike in elemental intensities.

Discussion

Electromagnetic conductivity surveys and XRF-based geochemical analysis of soil cores reveal strong relationships between spatial variations in sediment properties and apparent conductivity in the shallow subsurface. While apparent conductivities near the surface (e.g., as derived from 15 kHz signal energization) are uniformly low and reflect the rapidly-drained, massive aeolian sands covering the landscape, deeper apparent conductivities (e.g. from 5 and 3 kHz excitation) are generally higher but also more spatially variable across the study area. The higher variability of the lower-frequency

responses suggests an uneven nonconformity between modern aeolian sediments and a buried pre-Holocene surface. The varied depth of this nonconformity would inform vegetation assemblages and affect the observed highly divergent soil patterns across the relatively small study area.

The apparent conductivities measured using the 15 kHz signal are less spatially variable and bear little resemblance to topography and soils at the surface (see Fig. 15). In the (predominantly upwind) southeast quadrant of the study area near Core 6, there are higher apparent conductivities than to the northwest. This upwind portion of the study area is a deflation flat characterized by elevations that are 1 to 2 m lower than areas downwind of the active dunes. The average grain size measured from Core 6 is slightly higher than that measured from Core 5 (182 vs. 173 μm); however, topography seems to affect surface water flow more than infiltration dictated by variations in grain size. So, this difference would probably not be strong enough to affect apparent conductivity. We observed a perched water table at ~70 cm depth at this site while collecting cores in May after the relatively moist winter of 2014-2015, and there is an artesian well feeding a livestock pond at the central-eastern margin of the study area. These contextual observations imply a perched water table in the shallow subsurface, which probably resulted in the high apparent conductivities. An additional hot spot in apparent conductivity is located in the central-western margin of the study area near a maintained stock pond. Groundwater seeping from the pond most likely caused the higher conductivities observed there.

Apparent conductivities measured at 5 kHz show much higher spatial variation than those measured by the 15 kHz signal. Standard deviation of the deeper-probing

measurements is 11.7 mS/m, compared to 8.7 for those probing closer to the surface. Apparent conductivity variations are strongly associated with surface topographic features and soil properties as observed from XRF analysis. On the upwind deflation flats, higher apparent conductivities dominate while dune ridges display much lower conductivities (see Fig. 15). The hot spots in apparent conductivity observed from the 15 kHz signal persist at 5 kHz, implying a shallow water table across the study area that is closer to the surface in the deflated upwind flats. A large arc of low apparent conductivities dominates the central portion of the study area, and is associated with the contemporary migrating dune patch that is seen in visible imagery. The low conductivities observed here likely result from the relatively coarse grain sizes found on actively migrating dunes, and the rapid infiltration capacity of aeolian sands keeping the surface drier than at an equivalent depth in adjacent woodlands and prairie.

There is another area of lower apparent conductivity on the downwind side of the dunes that cannot be immediately explained by comparison with soil surveys, visible imagery, or elevation models. XRF analysis of Core 5, located adjacent to this zone of lower apparent conductivity, shows, via the high Si content, that aeolian sands dominate the subsurface. This core is located within the Nueces alfisol, in relatively low-lying ground in relict dune sands. The adjacent low apparent conductivity values are spatially associated with a Sarita alfisol, which is similar to the Nueces but occupies slightly higher ground (see Fig. 18). Each of these soils is expressed at the surface as a thick mantle of deep, massive aeolian sands. This particular area was previously identified as a relict dune ridge stabilized at the end of an earlier activation period than the present generation of

dune patches that are currently migrating across the study area (Barrineau et al., 2016). The larger grain sizes found on actively migrating dune ridges and resultant high infiltration capacity, coupled with the deep aeolian sands marking the edges of this relict landform, help to explain the lower conductivities. This explanation demonstrates the capability of EMI profilers to detect subtle but significant variations in moisture content and grain size.

Apparent conductivities measured by the 3 kHz signal are generally the highest of the three EMI datasets presented, and display a greater dynamic range. Average apparent conductivities are 18.0 mS/m with a standard deviation of 16.4 mS/m. Visualizations of apparent conductivity at this depth show a more fragmented pattern than those observed at shallower depths, but otherwise retain a similar spatial distribution. For example, the higher apparent conductivities observed across the upwind deflation flat are even higher, while the lower conductivity values beneath active and relict dune ridges are even lower.

There are two possible interpretations for the high dynamic range of the 3 kHz signal. The first is concerned with vegetation communities and their interactions with groundwater hydrology. Aeolian sands allow for rapid infiltration, and with little to no vegetation in place to slow or stop the percolation of surface water into the ground, these dryness of the sands tends to persist. The prairie and woodland vegetation (in particular tall grasses and honey mesquite) located around the southeastern, northeastern, and northwestern portions of the study area are capable of accessing groundwater several meters laterally and vertically, and could be extracting water from the dune ridges (Weaver and Zink, 1946; Nippert et al., 2011). Honey mesquite in particular is capable of adjusting

root growth patterns and depths to maximize water use during both humid and arid periods, and can affect the remaining groundwater that is available for native live oaks and prairies (Ansley et al., 2007).

A second possible interpretation is related to the geological framework. Previous research on the STSS suggests that the Holocene aeolian sands dominating the modern surface are mantled upon Pleistocene alluvium. The latter features a large fluvial network that could be derived from a paleo delta of either the Nueces River or Rio Grande (Price, 1958; Fisk, 1959; Bernard and Leblanc, 1965; Russell, 1981). The top of the Pleistocene material has been previously reported as varying in depth from 2-3 m to 8 m or more, and could feature individual paleo channels buried beneath aeolian sediments (Fisk, 1959; Forman et al., 2009). A 1-D inversion of the EMI surveys presented here suggests the thickness of the aeolian sands varies from < 1.0 m to in excess of 30 m. Cores extending deeper into the subsurface than those collected for this study are needed to confirm the depth to the Holocene-Pleistocene contact.

The variations in depth of the Holocene sands overlying the Pleistocene alluvium may be correlated if Holocene aeolian sands have filled the topographic lows left by the Pleistocene fluvial network. This process has been suggested through previous analysis of exploratory cores and seismic surveys on the Laguna Madre tidal flats adjacent to the STSS (see Fisk, 1959). Modern wells drilled for fresh water routinely exceed 500 ft depth in order to bypass smaller or more saline aquifers. So, groundwater extraction almost certainly bypasses the Pleistocene material and accesses a much deeper deposit (Dieterle and Vera, pers. comm., 2015). The distribution of shallower groundwater is likely affected

by the spatial distributions of relict fluvial channels in the subsurface, particularly within the depth range of this study (maximum layer thickness of 31.6 m). Therefore the variations in grain size of the Pleistocene alluvium and the differential deposition of aeolian sands above it may result in a series of fragmented, localized aquifers. Theses would be affected from below by the distribution of various fluvial grain sizes, and from above the rates of infiltration determined by variations in aeolian sediments.

## Conclusions

The results of this paper collectively demonstrate the utility and limitations of EMI profilers in measuring soil variations in semi-stabilized aeolian landscapes, and the value of contextual environmental information that may be gleaned from an EMI survey paired with analyzed core samples. However, it would not appear that EMI surveys are a magic bullet for detecting sub-surface variations in sediment strictly associated with periods of drought and/or humidity.

The data presented here show variations in apparent conductivity are spatially associated with surface grain size, moisture, and morphology. More specifically, EMI surveys reflect accumulations of water in the near subsurface related to specific grain size and morphodynamic conditions. The difficulty in using apparent conductivities to map aeolian sediments lies in determining which environmental factors are causing variations in apparent conductivity. While some studies have been able to establish a strong relationship between apparent conductivity and surface features like soils (Andre et al., 2011) and flood deposits from a single known event (Kitchen et al., 1993), these surveys were performed in a more controlled environment where external conditions are more well

known than across the STSS. Inter-seasonal surveys in a semi-stabilized dune system could be used to associate apparent conductivity with water table depth under different climate conditions. With this information, it would be much easier to determine whether or not perched water tables (and thus geologic framework) are over-riding surface infiltration patterns dictated by grain size and vegetation variations.

In spite of these issues, the continuity of data collected using EMI (bolstered by interpolating between closely-spaced survey points) makes these surveys quite valuable in verifying assumptions about shallow subsurface conditions across a relatively un-studied area. Making localized inferences about soil characteristics between coring sites, which traditionally are the primary source of information about subsurface properties, enables a greater degree of precision and accuracy in making landscape-scale conclusions about soil patterns. Future research using EMI profilers in the STSS and other semi-stabilized aeolian landscapes should focus on identifying characteristic apparent conductivities associated with distinct aeolian features that reflect specific process-form regimes. For example, do the associations between low conductivities and active dunes hold true through both drought and humid periods? Additionally, are differences in apparent conductivity at depth (e.g. high conductivity overlying low conductivity, and vice versa) associated with buried surfaces like paleo channels, or are these revealing shallow water tables created by variations in grain size resulting from different aeolian process regimes like grain fall deposits, migrating bedforms, or dust laminae?

This study illustrates the potential for identifying subsurface patterns associated with distinct periods of drought and humidity in aeolian landscapes. This relationship is

complicated by groundwater, which is influenced by morphology and grain size but also by precipitation. Since the surveys presented here were performed during a relatively moist period, it is somewhat difficult to absolutely determine whether or not observed apparent conductivities are affected more by climate or geologic framework. However, the spatial correlation between certain surface features suggests stratigraphy plays a significant role in interpreting EMI data.

# 4. DESERTIFICATION AND DUNE ACTIVITY IN SOUTH TEXAS

## Background

The South Texas Sand Sheet (STSS) is an extension of the West Gulf Coastal Prairie (EPA Level III No. 34) that lies across over roughly 10,000 $km^2$ between Corpus Christi and the Rio Grande (Forman et al., 2009; Griffith et al., 2004; Diamond and Fulbright, 1990; Diamond and Smeins, 1990; Fulbright et al., 1990; Fig. 20). The STSS is adjacent to the Laguna Madre wind flats and central Padre Island, and is composed almost entirely of Holocene aeolian sands derived from the adjacent tidal flats and barrier system overlying loamy Quaternary alluvium (Fig. 12). Winds are annually bimodal, with a dominant southeasterly flow during summer and a secondary northerly flow during winter (Texas Commission on Environmental Quality, 2008; see Fig. 12).

In the only published sedimentological analysis from the STSS, historic activations were dated at roughly 100 yr bp, 200 yr bp, 2000 yr bp, and 2700 yr bp (Forman et al., 2009). The most recent activation may correspond to the record-level 1950's drought (PDSI -4.2), while aridity and early settlement of the region with the introduction of livestock influenced the activation of dune systems during 1789-1790 AD (PDSI -3.8 and -4.7; Fulbright et al., 1990; Forman et al., 2009). The older activations are both associated with regional drought across the Southern High Plains and South Texas, suggesting a climate-controlled threshold in aridity associated with regional drying leads to desertification (Rich et al., 1999; Muhs and Zarate, 2001; Lepper and Scott, 2005; Miao et al., 2004; Forman et al., 2009).

The PDSI is based off parameterizations of precipitation, temperature, and soil moisture, and reflects departures in soil moisture from average conditions that last more than 3 to 6 months. As a result, it is primarily concerned with landscape scale drying. The PDSI scale is normalized such that zero is average, -2 is a moderate drought and <-4 is an extreme drought. Studies reconstructing PDSI conditions from dendrochronological and palynological evidence have found that sub decadal periods with PDSI < -2 are associated with enhanced dune activity across the Great Plains (Marin et al., 2005; Forman et al., 2006; Forman et al., 2008; Forman et al., 2009). By comparison, the 1950s drought that hammered South Texas is related to PDSI < -4 for three consecutive years and resulted in widespread desertification in the region (Fig. 11; Cook and Krusic, 2004; Cook et al., 2004). 20$^{th}$ century drought events have been compared to palaeo climate variability using metrics like the Palmer Drought Severity Index (PDSI), and found even that these 'droughts of record' pale in comparison to those experienced during the Medieval Warm Period and Holocene Altithermal Period, among others (see Cook et al., 2004). In South Texas, the PDSI exceeded -2 three times in the 20$^{th}$ century (Yu et al., 2006). For comparison, the PDSI in South Texas exceeded -2 between 1700 and 1900 12 times, and 22 times from AD 1000 to 1700 (Yu et al., 2006).

The sandy substrate of the STSS alters vegetation communities by promoting more diverse and extensive array of herbaceous forb vegetation than the Gulf Coastal Prairie (Fulbright et al., 1990). These herbaceous forb communities serve to distinguish the STSS from coastal prairies to the north and require more moisture than tallgrass prairies to maintain ground cover sufficient to reduce wind flow below threshold velocities for

aeolian transport. The STSS is located along a steep gradient between sub-humid and semi-arid climates such that annual rainfall decreases from over 800 mm to less than 600 mm in a span of less than 80 km and the Precipitation to Potential Evapotranspiration Ratio varies from 0.5 to 0.25, distinguishing this landscape from similar systems farther north (Johnston, 1963; Rappole et al., 1986; Diamond and Fulbright, 1990). The regional climate variability, along with the enhanced diversity and dominance of forbs, and enhanced evapotranspiration compared to other dune systems of the Great Plains, means the STSS is particularly vulnerable to desertification.

Dominant plant communities of the STSS are coastal tallgrass prairie dominated by inceptisols, sandy grasslands dominated by entisols, and patches of dense woody vegetation known as 'mottes' dominated by alfisols. This diverse mosaic of ground covers alters surface roughness, but active dunes often migrate over otherwise healthy and functioning grasslands and woodlands. Dead stands of live oak (*Quercus virginiana*) and honey mesquite (*Prosopois glandulosa*) remain in interdune areas as a testament to the inability of woody vegetation to fully stop dune advance, and are a common phenomenon across the STSS.

Historical accounts of the persistence of woody vegetation and shrublands suggest these communities may have been inadvertently nursed by settlement and the introduction of widespread ranching in the 18$^{th}$ and 19$^{th}$ centuries (Bartlett, 1854; O'Shea, 1935; Berlandier, 1980). Moreover the introduction of grazing livestock promotes the growth of honey mesquite that, if left to grow in dense thickets without continuous management, will eventually out-compete prairie grasses and lead to landscape degradation

(Heitschmidt et al., 1988; Archer, 1989; Ansley et al., 1997; Kramp et al., 1997). Surveys of the landscape performed by Manuel de Mier y Teran and Jean-Louis Berlandier funded by the Mexican government in the 19th century noted the persistence of wild horses and cattle across the region, abandoned by settlers in repeated population movements between northern Mexico and the United States (O'Shea, 1935; Berlandier, 1980).

These herds would have caused vegetation thinning in the native prairie that could have reduced surface roughness below the critical threshold needed to prevent aeolian transport, especially during periods of drought. Moreover the persistence of honey mesquite discourages the growth of tall grasses and tends to favor more sparse cover dominated by woody shrubs and cacti. At a landscape scale, this increases transport capacity by decreasing the density of leafy vegetation near the surface and makes the STSS more susceptible to desertification than before European settlement. However, it is difficult to quantify the degree to which livestock enhanced this vulnerability since there are not accurate records concerning the density of livestock or the estimated carrying capacity of native vegetation.

Methodology

**Soil Cores**

Guided by the results of Barrineau et al. (2016) and discussions with local experts to select sampling sites, soil cores were collected during the summer of 2015 (Fig. 21). The cores range in depth from 90 cm to 150 cm, and were collected manually using PVC pipe housing, a sledgehammer, and post-hole diggers. Cores 1, 2, 3, and 4 were collected along a topographic and pedological gradient where relict stabilized dunes and patchy active

dunes give way to dense mottes and more developed soils. Core 5 was collected immediately downwind of an actively migrating dune patch, while Cores 6 and 7 were collected in the upwind deflation basin of the same dune. Cores 8 and 9 were collected in the middle of extensive active and stabilized dunes with young soils, and Core 10 was collected in an area featuring continuous dense motte and more developed soils. Cores 1, 2, 3, 4, 5, 6, and 7 were collected in a line following prevailing winds along a northwest-southeast transect, while Cores 8 and 9 were collected to the south and west while Core 10 was collected to the north and east. Collectively, the locations of these samples are designed to maximize the amount of historical information on aeolian activation.

**XRF and Grain Size Analysis**

XRF core scanning is a useful technique for recording geochemical properties of sediment samples measured as a depth profile along a soil column. Samples are exposed to X-radiation that causes electrons to be ejected from inner atomic shells, and as electrons from the outer shells fill these vacancies they emit a pulse of X-radiation (Jenkins and DeVries, 1970). The energy and wavelength spectra of this emission, which vary based upon the element, are measured. The spectrum provides an estimation of elemental concentrations. XRF analysis can be used to generate environmental reconstructions based upon soil provenance and age (Jansen et al., 1998; Arz et al., 2001, 2003; Lamy et al., 2001; Andres et al., 2003; Weltje and Tjallingii, 2008).

XRF analysis requires that samples are prepared before laboratory testing and made as homogeneous and smooth as possible. Because split sediment cores will always contain variation in grain size, moisture, and shape, these conditions are incompatible with the

reality of analyzing field-collected core samples. Moreover, the results of XRF analysis will always be affected by the space between the scanner itself and the split core sample. X-radiation excited by the XRF system will compromise the measurement of many light elements, particularly those lighter than Si (Rothwell and Rack, 2006). Despite these weaknesses, XRF has become a widespread technique for analysis of cores in submarine as well as subaerial environments (Weltje and Tjallingii, 2008; Andres et al., 2003; Lamy et al., 2001; Arz et al., 2003, 2001; Jansen et al., 1998). The utility of XRF core scanners lies in their ability to deliver elemental *intensities* as raw data, despite theoretical drawbacks. Research focused on developing mass balance and flux data for the purposes of landscape modeling generally needs specific elemental *concentrations* to make output as robust as possible, but the *intensity* of elements within a split core is quite useful in its own right for qualitatively identifying heterogeneities in subsurface conditions. So, although there are possibilities for calibrating XRF results using linear and logarithmic transformations, for the purposes of this study elemental intensities are sufficient.

XRF analysis was performed on split cores in the Integrated Ocean Discovery Program (IODP) laboratory at Texas A&M University, using a third-generation Avaatech XRF Core Scanner. Cores were split, separated, and sampled at 1 cm intervals. Excitation was performed at 10 and 30 kV, and measured elemental intensities for major elements between Al and U. Because we are using these cores to qualitatively identify specific soil series across the study area, as opposed to mass balance or flux modeling of sediment transport pathways and/or provenance, elemental intensities are sufficient and we did not

pursue more complex calibrations of measurements in order to calculate elemental concentrations.

Grain size measurements were collected in the laboratory using a Horiba Camsizer, which digitally imaged and analyzed thousands of particles for each sample. Samples were collected from split cores at 10 cm intervals and run through the camsizer for 5 minutes each. Detection limits for the camsizer were selected from standard Wentworth scale sediment grain sizes, ranging from 0.063 mm – 0.5 mm, and distributions were collected at $10^{th}$, $50^{th}$, and $90^{th}$ percentiles. Average grain sphericity was collected across all grain sizes for each sample point as well.

**Optically-Stimulated Luminescent Dating**

OSL-derived dates have been used in a number of studies examining environmental histories in the Great Plains (Stokes and Swinehart, 1997; Goble et al., 2004; Forman et al., 2006; Halfen and Johnson, 2013) as well as other aeolian and coastal environments (Arbogast et al., 2002; Bristow and Pucillo, 2006; Thomas and Wiggs, 2008; Clemensen et al., 2009), and have yielded optical ages consistent with $^{14}C$ ages and historic observations (see Forman et al., 2009). OSL analysis uses luminescent emissions to measure time elapsed since the last light exposure for a sample, which makes it particularly useful in aeolian environments where the last light exposure represents the date of deposition and incorporation in the subsurface (Aitken, 1998; Forman et al., 2009).

Soil cores containing samples used for OSL analysis at a Baylor University laboratory were painted black and covered with solid opaque tape before being collected in order to avoid light contamination. We used an Automated Risø TL/OSL-DA-20 system (Bøtter-

Jensen, 2000) for single aliquot measurements. Blue light excitation (470 +/- 30 nm) is from an array of 30 light-emitting diodes that deliver approximately 25 $mW/cm^2$ to the sample position at 90% power. A Thorn EMI 9235 QA photomultiplier tube coupled with three 3-mm-thick Hoya U-340 detection filters that transmit between 290 and 370 nm was used to measure photon emissions. Laboratory irradiations use a calibrated $^{90}Sr/^{90}Y$ beta source coupled with the Risø reader and the experimental sequences are executed using Risø TL/OSL software for MS-Windows. Emissions are integrated over the first 0.8 s of stimulation out of 400 s of measurement, with background based on emissions for the last 75- to 100-second interval. Previous research using samples from this study area used a similar OSL methodology and found excellent reproducibility in results (see Forman et al., 2009).

Results

**Grain Size Data**

Grain size analysis show variations from very fine sands to very fine pebbles, with $D_{50}$=166 µm. Previous observations show theses aeolian sands are primarily massive with little internal cross stratification (see Forman et al., 2009). In general, there are relatively lower average grain sizes in areas with rugged topography and younger soils compared to areas with little topography and more horizonation (182 µm vs. 202 µm). Moreover, in these younger soils the standard deviation of $D_{50}$ is much smaller (6.2 µm vs. 19.3 µm).

**XRF Analysis**

XRF data reveal strong associations between collected data and six localized soil series across the study area. Sites exhibiting little horizonation tended to be located in areas with

more evidence of recent aeolian activity, and are correlated with the Falfurrias, Potrero, and Arenisco entisols (Fig. 22). Sites along the margins of recently active dunes revealed more enhanced horizonation and are correlated with the Topo inceptisol (Fig. 23). Sites located in topographically featureless areas with extensive woody vegetation exhibited the most horizonation and are correlated with the Nueces and Sarita alfisols (Fig. 24).

The variations between these soil orders are primarily evidenced through changes in subsurface geochemistry (or the lack thereof) at sampling sites. In the entisol samples there is little evidence of horizonation outside localized variations in Si intensities, which are hypothesized to represent distinct episodes of aeolian accumulation associated with periodic dune activity (Fig. 25). The inceptisols tend to exhibit little horizonation other than strong inverse relationships between Si and Ca, where the cores show sudden increases in Ca content associated with relatively larger grain sizes that may be influenced by cementation from carbonate muds common in the study area. The alfisols show enhanced horizonation via greater variations in Si content along with higher intensities of nearly every other element measured by the XRF scanner.

**OSL Dates**

Based upon initial XRF results and previous chronologies of the STSS, 3 cores were selected for OSL analysis (Fig. 21). Using a space for time substitution, Cores 5 and 8 are the representative members of soil characteristics on the upwind and downwind margins of actively migrating dune systems. Core 10 is used as a representative sample of much older aeolian sediments with little evidence for recent dune activity. Horizons used for sampling were selected based upon grain size and elemental intensity variations

representing the final stages of dune activity at the three locations. The parameters of the OSL analysis and resultant dates are provided in Table 1.

At Core 5, a contact between distinct unmodified aeolian A-horizons at 15 cm depth was used as a proxy for the most recent episode of dune activity at this site. A C-horizon underlying the surficial aeolian sands at around 100 cm depth was used as a proxy for the initiation of dune activity (see Fig. 22). The 15 cm A1-A2 contact was dated at 75±7 yr bp, while the 100 cm A-C contact was dated at 4125±300 yr bp.

At Core 8, multiple stacked aeolian A-horizons without pedogenesis represent distinct periods of dune activity with buried A horizons at 15 and 40 cm depth, and a C-horizon at 100 cm depth (see Fig. 23). The 15 cm A1-A2 contact was dated at 235±20 yr bp, and the 100 cm A-C contact was dated at 1935±140 yr bp.

At Core 10, an E-horizon lies between the surficial A-horizon, at roughly 35 cm depth, and a C-horizon at roughly 95 cm depth (see Fig. 24). The A-E contact, representing the most recent generation of sediment deposition at the site, was dated at 230±25 yr bp, while the E-C horizon representing the initiation of aeolian activity was dated at 6560±460 yr bp.

## Discussion

These data contribute to the existing conceptual model of Holocene-scale dune activity across the STSS by reinforcing previous findings (see Forman et al., 2009) and introducing two new activations in need of further investigation. Additionally, future work is needed on the long-term relationship between the STSS and the adjacent Laguna Madre and Padre Island systems. Aeolian activations are dated at ca. 75, 230, 2000, 4100, and 6600 yr bp.

Activations at 75, 230, and 2000 yr bp are consistent with previously published chronologies from the STSS (Forman et al., 2009). Activations at 4100 and 6600 yr bp are less well-examined, but there are possibilities for regional drought and changes in geological framework leading to widespread dune activity at these dates. Considered holistically, the activation periods presented herein are derived from a mixture of influences.

Dune activity associated with ca. 75 yr bp is related to regional shifts in climate leading to enhanced aridity. Extreme droughts were observed in the South Texas plains at decadal intervals from 1920 to 1950, with PDSI values exceeding -4.33 three years consecutively in the early 1950s (Yu et al., 2006; Forman et al., 2009). Additionally, modern soil conservation techniques designed to prevent soil loss and land degradation were not yet implemented until the middle of the 20$^{th}$ century. So, it appears that a mixture of sequential drought and a certain level of anthropogenic disturbance is capable of inducing dune activation across the system. Historical aerial imagery of the study area from 1952, in the midst of the droughts, shows nearly continuous migrating dunes stretching across wide swaths of land now occupied by prairie grasses and woodlands (Fig. 11).

An activation at ca. 230 yr bp is also similar to previous chronological results from the STSS (Forman et al., 2009). This activation was detected at two of the sample sites (Cores 8 and 10) featuring vastly different modern environments. Core 8 is located on a low relict dune ridge in a large prairie featuring hummocky topography and actively migrating dunes, while Core 10 is located amongst dense wooded flats away from any modern or relict dune landform (Fig. 25). The disparity in modern biophysical setting but

synchronicity in activation periods suggests two potential explanations. First, there could have been a drought that induced dune migration and aeolian deflation across the entire landscape and the modern surface was fundamentally shaped by this event. This is a possibility, as AD 1789 and 1790 experienced droughts with PDSI of -4.26 in South Texas, which compared to the 1950s drought and imagery would have resulted in widespread desertification (Yu et al., 2006; Forman et al., 2009). Second, there could have been another control influencing the degree of desertification that made the landscape particularly susceptible to localized dune activity that may have been effaced into the modern landscape long enough to be difficult to determine today. This is also a possibility, as the 1790s and 1800s was the period in which the Spanish and Mexican governments established large land grants and introduced horses to South Texas (Coole 1952; Lehmann, 1984; Fulbright et al., 1990).

Observed activations at ca. 4100 and 6600 yr bp suggest the STSS is much older than discussed in previous research (Forman et al., 2009). The ca. 4100 yr bp activation period correlates with dune activity observed in Oklahoma (Lepper and Scott, 2005), and in the Northern Plains and Canada (Mensing et al., 2004; Halfen and Johnson, 2013). There is little evidence beyond these three instances suggesting this particular event is associated with widespread regional desertification across the Great Plains. On the other hand, several types of historical data including fluvial sedimentation records (Simms et al., 2010; Anderson et al., 2014), $^{14}C$ samples (Wilkins and Currey, 1999), palynological analyses (Nordt et al., 1994) suggest the Texas climate experienced an optimum period of warmth and aridity driven by synoptic atmospheric and oceanic circulation between ca. 7500 and

3500 yr bp. There is also evidence suggesting the rate of sea level rise on the Texas coast slowed from 1.4 mm/yr to around 0.5 mm/yr around 4000 yr bp, which may have allowed for accumulation of aeolian sediments on the low-lying coastal plain now mantled by the STSS (Anderson et al., 2016). A radiocarbon dated contact between shell fragments and beach-dune sediments on neighboring Padre Island suggests the ca. 4000 yr bp event may be synchronous with creation of the beach dune system on the barrier, but this is difficult to confirm without further research (see Fisk, 1959).

Activations at ca. 6600 yr bp are the oldest dated deposits from the STSS and suggest it is an older landform than most modern barriers in the region (Anderson et al., 2016). This particular activation is correlated with widespread dune activity and desertification in Alberta (Vance et al., 1992), Saskatchewan (Wolfe et al., 2006), Manitoba (Wolfe et al., 2000), the Northern and Central Great Plains (Mensing et al., 2004; Miao et al., 2007; Halfen et al., 2010; Grimm et al., 2011; Halfen and Johnson, 2013), and the Southern High Plains of Texas and New Mexico (Holliday, 1997; Frederick, 1998; Grissino-Mayer, 1996; Hall and Penner, 2012). The disparate climates and biophysical environments that experience desertification during this period suggest this particular episode was driven by synoptic scale changes in climate and circulation. The middle Holocene climatic optimum, or 'altithermal', resulted in a peak in global temperatures around 6000 yr bp. Slight variations in this pattern would be expected at the regional scale, and the climatic optimum identified for Texas occurred between ca. 7500 and 3500 yr bp (Weight et al., 2011).

Modern projections suggest anthropogenic climate change will induce decreases in moisture availability throughout the Great Plains (Cook et al., 2004). This brings the two-

fold impact of decreased precipitation as well as increased evapotranspiration. As a result, surface systems that are already susceptible to drought variability will be placed under significantly more stress encouraging regional desertification. The existing conceptual model of the Holocene evolution of the STSS identifies climate stresses as the primary determinant of dune activation patterns, but results presented herein introduce the possibility of connections between specific degrees of anthropogenic and ecological stresses and dune activity, and the relationship between geological framework and modern desertification vulnerability. Moreover these results extend the time scale of aeolian activity in the STSS an additional three millennia beyond published OSL dates. This study demonstrates how a mixture of methods can be used to augment the final results of field-based investigations in semi-stabilized dune systems on the Great Plains by developing a data-driven sampling scheme for core sites in order to theoretically maximize historical information contained in the shallow subsurface.

# 5. CONCLUSIONS

The STSS is the southernmost extension of a series of dune systems scattered across the Great Plains from Canada to Mexico. These systems react to variations in moisture and ecological stress through dune activation and stabilization cycles that have occurred repeatedly throughout the Holocene. Results presented here suggest the STSS is much older than previously thought, and there is evidence of multiple landscape-scale controls on dune activation including climate variability, geologic framework, and human activity. Drought causes a reduction in vegetation density at the surface, increasing the transport capacity of the persistent southeasterly winds across the STSS. Multiple dated activation periods are contemporaneous with regional-scale drying observed in systems further north. The oldest dated samples presented were deposited at roughly the same time Padre Island may have become a relatively continuous barrier. This would have shut of Laguna Madre from the Gulf of Mexico and likely triggered the creation of the modern wind flats between the island and STSS, but this is difficult to confirm without more detailed information from the lagoon and island. The introduction of livestock following European settlement changed the vegetation communities across the STSS and caused an increase in woody shrub and cactus growth at the expense of leafy, herbaceous vegetation.

Collectively, each of these three controls appear to have caused periods of desertification in South Texas during the Holocene. However, these correlations are difficult to prescribe as causative without direct observations or more rigorous historical analyses. Future work is needed in order to tie together the Holocene histories of Padre

Island, Laguna Madre, and the STSS, as well as in order to identify specific regional thresholds in moisture associated with reductions in vegetation that can lead to desertification. If these two lingering questions – the specific relationship between the adjacent coastal systems and the STSS, and the precise thresholds at which drought can induce desertification – can be addressed, a computational model of landscape evolution could be developed and compared to other semi-stabilized dune systems across the Great Plains.

# REFERENCES


Alley, W., 1984. The Palmer Drought Severity Index: limitations and assumptions. Journal of Climate and Applied Meteorology 23, 1100-1109.

Anderson, J., Wallace, D., Simms, A., Rodriguez, A., Milliken, K., 2014. Variable response of coastal environments of the northwestern Gulf of Mexico to sea level rise and climate change: implications for future change. Marine Geology 352, 348-366.

Anderson, J., Wallace, D., Simms, A., Rodriguez, A., Weight, R., Taha, P., 2016. Recycling sediments between source and sink during a eustatic cycle: systems of late Quaternary northwestern Gulf of Mexico Basin. Earth Science Reviews 153.

Andre, F., van Leeuwen, C., Saussez, S., Van Durmen, R., Bogaert, P., Moghadas, D., Resseguier, L., Delvaux, B., Vereecken, H., Lambot, S., 2012. High-resolution imaging of a vineyard in south of France using ground-penetrating radar, electromagnetic induction and electrical resistivity tomography. Journal of Applied Geophysics 78, 113-122.

Andres, M., Bernasconi, S., McKenzie, J., Rohl., U., 2003. Southern Ocean deglacial record supports global Younger Dryas. Earth and Planetary Science Letters 216, 515-525.

Ansley, J., Huddle, J., Kramp B., 1997. Mesquite ecology. Texas Agricultural Experiment Station, Vernon, TX. Web site: http://texnat.tamu.edu/library/symposia/brush-sculptors-innovations-for-tailoring-brushy-rangelands-to-enhance-wildlife-habitat-and-recreational-value/mesquite-ecology/.

Ansley, J., Castellano, M., 2007. Prickly pear cactus responses to summer and winter fires. Rangeland Ecology and Management 60(30), 244-252.

Arbogast, A., Hansen, E., Van Oort, M., 2002. Reconstructing the geomorphic evolution of large coastal dunes along the southeastern shore of Lake Michigan. Geomorphology 46, 241-255.

Archer, S., 1989. Have Southern Texas savannas been converted to woodlands in recent history? The American Naturalist 134, 545-561.

Archer, S., Smeins, F., 1991. Ecosystem-level processes. In: Rodney, K., Stuth, J., (Eds.) Grazing management an ecological perspective. Timber Press, Portland, Oregon.

Arz, H., Gerhardt, S., Patzold, J., Rohl, U., 2001. Millennial-scale changes of surface- and deep-water flow in the western tropical Atlantic linked to Northern Hemisphere high-latitude climate during the Holocene. Geology 29, 239-242.

Arz, H., Patzold, J., Muller, P., Moammar, M., 2003. Influence of Northern Hemisphere climate and global sea level rise on the restricted Red Sea marine environment during termination I. Paleoceanography 18.

Ashkenazy, Y., Yizhaq, H., Tsoar, H., 2012. Sand dune mobility under climate change in the Kalahari and Australian deserts. Climatic Change 112, 901-923.

Baas, A., Nield, J., 2010. Ecogeomorphic state variables and phase-space construction for quantifying the evolution of vegetation aeolian landscapes. Earth Surface Processes and Landforms 35, 717-731.

Barbosa, R., Overstreet, C., 2011. What is electrical conductivity? Publication 3185, Louisiana State University AgCenter Research & Extension.

Barrineau, P., Dobreva, I., Bishop, M., Houser, C., 2016. Deconstructing a polygenetic landscape using multi-resolution analysis and LiDAR. Geomorphology 258, 51-67.

Bartlett, J., 1854. Personal narrative of explorations and incidents in Texas, New Mexico, California, Sonora and Chihuahua. D Appleton & Co., New York. 2 Vols.

Bernard, H., Leblanc, L., 1965. Resume of the Quaternary geology of the northwestern Gulf of Mexico province. In: Wright, H., Frey, D. (Eds.), The Quaternary of the United States. Princetno University Press, Princeton, New Jersey, 137-185.

Bhattachan, A., D'Odorico, P., Dintwe, K., Okin, G., Collins, S., 2014. Resilience and recovery potential of duneland vegetation in the southern Kalahari. Ecosphere 5.

Bishop, M., James, A., Shroder, J., Walsh, S., 2012. Geospatial technologies and digital geomorphological mapping: concepts, issues and research. Geomorphology 137, 5-26.

Bøtter-Jensen, L., Bulur, E., Duller, G., Murray, A., 2000. Advances in luminescence instrument systems. Radiation Measurements 32, 523-528.

Breña-Naranjo, J., Kendall, A., Hyndman, D., 2014. Improved methods for satellite-based groundwater storage estimates: a decade of monitoring the high plains aquifer from space and ground observations. Geophysical Research Letters 41, doi:10.1002/2014GL061213

Bristow, C., Pucillo, K., 2006. Quantifying rates of coastal progradation from sediment volume using GPR and OSL: the Holocene fill of Guichen Bay, southeast South Australia. Sedimentology 53(4), 769-788.

California Soil Resource Lab, 2014. SoilWeb Earth. University of California-Davis, Department of Land, Air, and Water Resources. URL: http://casoilresource.lawr.ucdavis.edu/soilweb-apps. Accessed November 15 2014.

Clark, J., Grimm, E., Donovan, J., Fritz, S., Engstrom, D, Almendinger, J., 2002. Drought cycles and landscape responses to past aridity on prairies of the northern Great Plains, USA. Ecology 83(3) 595-601.

Clemmensen, L., Murray, A., Heinemeier, J., De Jong, R., 2009. The evolution of Holocene coastal dunefields, Jutland, Denmark: a record of climate change over the past 5000 years. Geomorphology 105, 303-313.

Coleou, T., Poupon, M., Azbel, K., 2003. Interpreter's corner – unsupervised seismic facies classification: a review and comparison of techniques and implementation. The Leading Edge 22, 942-953.

Cook, E., Woodhouse, C., Eakin, C., Meko, D., Stahle, D., 2004. Long-term aridity changes in the Western United States. Science 306, 1015-1018.

Cook, E., Krusic, P., 2004. The North American drought atlas. Lamont-Doherty Earth Observatory and the National Science Foundation.

Cordova, C., Porter, J., Lepper, K., Kalchgruber, R., Scott, G., 2005. Preliminary assessment of sand dune stability along a bioclimatic gradient, north-central and northwestern Oklahoma. Great Plains Research 15, 227-249.

Corwin, D., Lesch, S., 2005. Characterizing soil spatial variability with apparent soil electrical conductivity II: case study. Computers and Electronics in Agriculture 46(1-3), 135-152.

Darrenougue, N., De Deckker, P., Fitzsimmons, K., Norman, M., Reed, L., van der Kaars, S., Fallon, S., 2009. A late Pleistocene record of aeolian sedimentation in Blanche Cave, Naracoorte, South Australia. Quaternary Science Reviews 28, 2600-2615.

Diamond, D., Fulbright, T., 1990. Contemporary plant-environments of upland grasslands of the coastal sand plain, Texas. Southwestern Naturalist 35, 385-392.

Diamond, D., Smeins, F., 1990. Remnant grassland vegetation and ecological affinities of the upper coastal prairie of Texas. The Southwestern Naturalist 29(3), 321-334.

Dieterle, W., Vera, H., 2015. Personal communication, Kenedy Memorial Foundation offices, Sarita, TX.

Everett, M., 2012. Theoretical developments in electromagnetic induction geophysics with selected applications in the near surface. Survey Geophysics 33, 29-63.

Fisk, H., 1959. Padre Island and Laguna Madre Flats, coastal South Texas. Second Coastal Geography Conference, Coastal Studies Institute, Louisiana State University, Baton Rouge, LA, April 6-9, 1959.

Forman, S., Oglesby, R., Webb, R., 2001. Temporal and spatial patterns of Holocene dune activity on the Great Plains of North America: megadroughts and climate links. Global and Planetary Change 29, 1-29.

Forman, S., Marin, L., Pierson, J., Gomez, J., Miller, G., Webb, R., 2005. Eolian sand depositional records from western Nebraska: landscape response to droughts in the past 1500 years. The Holocene 15, 973-981.

Forman, S., Marin, L., Gomez, J., Pierson, J., 2008. Late Quaternary eolian sand depositional record for southwestern Kansas: landscape sensitivity to droughts. Palaeogeography Palaeoclimatology Palaeoecology 265, 107-120.

Forman, S., Nordt, L., Gomez, J., Pierson, J., 2009. Late Holocene dune migration on the south Texas sand sheet. Geomorphology 108, 159-170.

Frederick, C., 1998. Late Quaternary clay dune sedimentation on the Llano Estacado, Texas. Plains Anthropologist 43, 137-155.

Fryberger, S., Dean, G., 1979. Dune forms and wind regime. In: McKee, E. (Ed.), A study of Global Sand Seas. Professional Paper 1052, U.S. Geological Survey, 137-169.

Fulbright, T., Diamond, D., Rappole, J., Norwind, J., 1990. The coastal sand plain of southern Texas. Rangelands 12(6), 337-340.

Fung, T., LeDrew, E., 1987. Application of principal components analysis to change detection. Photogrammetric Engineering and Remote Sensing 53(12), 1649-1658.

Geophysical Survey Systems, Incorporated., 2007. Profiler EMP-400 user manual.

Goble, R., Mason, J., Loope, D., Swinehart, J., 2004. Optical and radiocarbon ages of stacked paleosols and dune sands in the Nebraska Sand Hills, USA. Quaternary Science Reviews 23(9-10), 1173-1182.

Griffith, G., Bryce, S., Omernik, J., Comstock, J., Rogers, A., Harrison, B., Hatch, S., Bezanon, D., 2004. Ecoregions of Texas. U.S. Environmental Protection Agency, Corvallis, OR.

Grimm, E., Donovan, J., Brown, K., 2011. A high-resolution record of climate variability and landscape response from Kettle Lake, northern Great Plains, North America. Quaternary Science Reviews 19-20, 2626-2650.

Grissino-Mayer, H., 1996. A 2129-year reconstruction of precipitation for northwestern New Mexico, USA. In: Dean, J., Meko, D., Swetnam, T. (Eds.), Tree rings, environment, and humanity. Arizona, Radiocarbon, Tucson, 191-204.

Grisso, R., Alley, M., Holshouser, D., Thomason, W., 2006. Precision farming tools: soil electrical conductivity. Virginia Cooperative Extension publication 442.

Grunsky, E., 2002. The application of principal components analysis to multi-beam RADARSAT-1 satellite imagery: a tool for land cover and terrain mapping. Canadian Journal of Remote Sensing 28(6), 758-769.

Guitet, S., Cornu, J., Brunaux, O., Betbeder, J., Carozza, J., Richard-Hansen, C., 2013. Landform and landscape mapping, French Guiana (South America). Journal of Maps 9(3), 325-335.

Guo, H., Marfurt, K., Liu, J., 2009. Principal component spectral analysis. Geophysics 74(4), 35-43.

Halfen, A., Fredlund, G., Mahan, S., 2010. Holocene stratigraphy and chronology of the Casper dune field, Casper, Wyoming, USA. The Holocene 20, 773-785.

Halfen, A., Johnson, W., 2013. A review of Great Plains dune field chronologies. Aeolian Research 10, 135-160.

Hall, S., Penner, W., 2012. Stable carbon isotope, $C_3$-$C_4$ vegetation, and 12,800 years of climate change in central New Mexico, USA. Palaeogeography, Palaeoclimatology, Palaeoecology 369, 272-281.

Haschke, M., 2006. The Eagle III BKA system, a novel sediment core X-ray fluorescence analyzer with very high spatial resolution. In: Rothwell, R. (Ed.), New Techniques in Sediment Core Analysis. Special Publication, 267. Geological Society, London, 31-37.

Heitschmidt, R., Ansley, J., Dowhower, S., Jacoby, P., Price, D., 1988. Some observations from the excavation of honey mesquite root systems. Journal of Range Management 41, 227-231.

Haug, G., Gunther, D., Peterson, L., Sigman, D., Hughen, K., Aeschlimann, B., 2003. Climate and the collapse of Maya civilization. Science 299, 1731-1735.

Holliday, V., 1989. Middle Holocene drought on the southern High Plains. Quaternary Research 31, 74-82.

Holliday, V., 1997. Origin and evolution of lunettes on the High Plains of Texas and New Mexico. Quaternary Research 47, 54-69.

Houser, C., Hapke, C., Hamilton, S., 2008. Controls on coastal dune morphology, shoreline erosion and barrier island response to extreme storms. Geomorphology 100(3-4), 223-240.

Houser, C., Hamilton, S., 2009. Sensitivity of post-hurricane beach and dune recovery to event frequency. Earth Surface Processes and Landforms 34(5), 613-628.

Houser, C., Wernette, P., Rentschlar, E., Jones, H., Hammond, B., Trimble, S., 2015. Post-storm beach and dune recovery: implications for barrier island resilience. Geomorphology 234, 54-63.

Huang, H., Won, I., 2000. Conductivity and susceptibility mapping using broadband electromagnetic sensors. Jounral of Environmental and Engineering Geophysics 5(4), 31-41.

Huang, H., Rudd, J., 2008. Conductivity-depth imaging of helicopter-borne TEM data based on a pseudolayer half-space model. Geophysics 73, F115-F120.

Hugenholtz, C., Wolfe, S., 2005a. Biogeomorphic model of dunefield activation and stabilization on the northern Great Plains. Geomorphology 70, 53-70.

Hugenholtz, C., Wolfe, S., 2005b. Recent stabilization of active sand dunes on the Canadian prairies and relation to recent climate variations. Geomorphology 68, 131-147.

Hugenholtz, C., Levin, N., Barchyn, T., Baddock, M., 2012. Remote sensing and spatial analysis of aeolian sand dunes: a review and outlook. Earth-Science Reviews 111, 319-334.

Jansen, J., Van der Gaast, S., Koster, B., Vaars, A., 1998. COTEX, a shipboard XRF-scanner for element analysis in split element cores. Quaternary Research 151, 143-153.

Jenkins, R., DeVries, J., 1970. Worked examples in X-ray analysis. Macmillan: London.

Jensen, J., 2005. Introductory digital image processing: a remote sensing perspective. Prentice Hall: Upper Saddle River, NJ.

Johnston, M., 1963. Past and present grasslands of Southern Texas and Northeastern Mexico. Ecology 44, 456-466.

Kramp, B., Ansley, J., Tunnell, T., 1998. Mesquite seedling survival from cattle and wildlife feces in a semi-arid grassland. Southwestern Naturalist 43, 300-312.

Kuriyama, Y., Lee, J., 2001. Medium-term beach profile change on a bar-trough region at Hasaki, Japan, investigated with complex principal component analysis. ASCE Coastal Sediments ’01, 959-968.

Kustu, D., Fan, Y., Robock, A., 2010. Large-scale water cycle perturbation due to irrigation pumping in the US High Plains: a synthesis of observed streamflow changes. Journal of Hydrology 390, 222-244.

Lamy, F., Kaiser, J., Ninnemann, U., Hebbeln, D., Arz, H., Stoner, J., 2001. Holocene rainfall variability in southern Chile: a marine record of latitudinal shifts of the Southern Westerlies. Earth Planetary Science Letters 185, 369-382.

LeHouerou, H., Norwine, J., 1988. The ecoclimatology of south Texas. In: Whitehead, E. (Ed.), Arid lands: today and tomorrow. Westview Press, Boulder CO, 417-433.

Lepper, K., Scott, G., 2005. Late Holocene aeolian activity in the Cimarron River valley of west-central Oklahoma. Geomorphology 70, 42-52.

Loope, D., Swinehart, J., 2000. Thinking like a dune field: geologic history in the Nebraska Sand Hills. Great Plains Research 10, 5-35.

Madole, R., 1994. Stratigraphic evidence of desertification in the west-central Great Plains within the past 1000 yr. Geology 22, 483-486.

Marin, L., Forman ,S., Valdez, A., Bunch, F., 2005. Twentieth century dune migration at the Great Sand Dunes National Park and Preserve, Colorado, relation to drought variability. Geomorphology 70, 163-183.

Mason, J., Swinehart, J., Goble, R., Loope, D., 2004. Late-Holocene dune activity linked to hydrological drought, Nebraska Sand Hills, USA. The Holocene 13, 209-217.

Mason, J., Lu, H., Zhou, Y., Miao, X., Swinehart, J., Liu, Z., Goble, R., Yi, S., 2009. Dune mobility and aridity at the desert margin of northern China at a time of peak monsoon strength. Geomorphology 37, 947-950.

Mason, J., Swinehart, J., Goble, R., Loope, D., 2004. Late-Holocene dune activity linked to hydrological drought, Nebraska Sand Hills, USA. The Holocene 13, 209-217.

Mensing, S., Benson, L., Kashgarian, M., 2004. A Holocene pollen record of persistent droughts from Pyramid Lake, Nevada, USA. Quaternary Research 62, 29-38.

Miao, X., Mason, J., Swinehart, J., Loope, D., Hanson, P., Goble, R., Xiaodong, L., 2007. A 10000 year record of dune activity, dust storms, and severe drought in the central Great Plains. Geology 35, 119-122.

Muhs, D., Maat, P., 1993. The potential response of eolian sands to greenhouse warming and precipitation reduction on the Great Plains of the U.S.A. Journal of Arid Environments 25, 351-361.

Muhs, D., Volliday, V., 1995. Evidence of active dune sand on the Great Plains in the 19th century from accounts of early explorers. Quaternary Research 43, 198-208.

Muhs, D., Stafford, T., Cowherd, S., Mahan, S., Kihl, R., Maat, P., Bush, C., Nehring, J., 1996. Origin of the late Quaternary dune fields of northeastern Colorado. Geomorphology 17, 129-149.

Nationwide Environmental Title Research, 2015. Historic Aerials. 2009-2015. Nationwide Environmental Title Research. Tempe, AZ. 15 December 2014.

Nippert, J., Ocheltree, T., Skibbe, A., Kangas, L., Ham, J., Arnold, K., Brunsell, N., 2011. Linking plant growth responses across topographic gradients in tallgrass prairie. Oecologia 166, 1131-1142.

Nordt, L., Boutton, T., Hallmark, C., Waters, M., 1994. Late Quaternary climate changes in Central Texas based on the isotopic composition of organic carbon. Quaternary Research 41, 109-120.

Norwine, J., Bingham, R., Zepeda, V., 1978. Twentieth century semiarid climates and climatic fluctuations in Texas and Northeastern Mexico. Journal of Arid Environment 1, 313-325.

Norwine, J., Bingham, R., 1986. Frequency and severity of droughts in South Texas: 1900-1983. In: Braun, R. (Ed.), Livestock and wildlife management during drought. Cesar Kleberg Wildlife Research Institute, Texas A&I University: Kingsville, Texas.

O'Shea, E., 1935. El Mesquite: a story of the early Spanish settlements between the Nueces and the Rio Grande. Texas A&M University Press: College Station, Texas.

Palmer, W., 1968. Keeping track of crop moisture conditions nationwide: the new crop moisture index. Weatherwise 21, 151-161.

Plant, N., Griggs, G., 1992. Interactions between nearshore processes and beach morphology near a seawall. Journal of Coastal Research 8(1), 183-200.

Price, W., 1958. Sedimentology and Quaternary geology of south Texas. Gulf Coast Association Geological Society Transactions 3, 41-75.

Rappole, J., Russell, C., Norwine, J., Fulbright, T., 1986. Anthropogenic pressures and impacts on marginal, neotropical, semi-arid ecosystems: the case of south Texas. Journal of Science Total Environment 55, 91-99.

Reisner, M., 1986. Cadillac Desert: the American west and its disappearing water. Viking Publishers: New York.

Rich, J., Stokes, S., Wood, W., 1999. Holocene chronology for lunette dune deposition on the Southern High Plains, USA. Zeitschrift fur Geomorphologie, supplementband 176, 165-180.

Robinson, D., Lebron, I., Kocar, B., Phan, K., Sampson, M., Crook, N., Fendorf, S., 2009. Time-lapse geophysical imaging of soil moisture dynamics in tropical deltaic soils: an aid to interpreting hydrological and geochemical processes. Water Resources Research 45, 2008WR006984.

Rodarmel, C., Shan, J., 2002. Principal component analysis for hyperspectral image classification. Surveying and Land Information Science 62, 115-122.

Rothwell, R., Rack, F., 2006. New techniques in sediment core analysis: an introduction. In: Rothwell, R. (Ed.), New techniques in sediment core analysis. Special Publication 267, Geological Society, London 1-29.

Russell, J., 1981. The south Texas eolian sand sheet. In: Russell, J., Sterling, C. (Eds.), Modern depositional environments of sands in South Texas. Gulf Coast Association of Geological Societies, Corpus Christi, Texas 43-46.

Sridhar, V., Loope, D., Swinehart, J., Mason, J., Oglesby, R., Rowe, C., 2006. Large wind shift on the Great Plains during the Medieval Warm Period. Science 313(5785), 345-347.

Stegner, W., 1954. Beyond the hundredth meridian: John Wesley Powell and the second opening of the American West. Houghton Mifflin: Boston.

Stokes, S., Swinehart, J., 1997. Middle- and late-Holocene dune reactivation in the Nebraska Sand Hills, USA. The Holocene 7, 263-272.

Sudduth, K., Kitchen, N., Wiebold, W., Batchelor, W., Bollero, G, Bullock, D., Clay, D., Palm, H., Pierce, F., Schuler, R., Thelen, K., 2005. Relating apparent electrical conductivity to soil properties across the north-central USA. Computers and Electronics in Agriculture 46, 263-283.

Sudduth, K., Myers, B., Kitchen, N., Drummond, S., 2013. Modeling soil electrical conductivity-depth relationships with data from proximal and penetrating $EC_a$ sensors. Geoderma 199, 12-21.

Telfer, M., Bailey, R., Burrough, S., Stone, A., Thomas, D., Wiggs, G., 2010. Understanding linear dune chronologies: insights from a simple accumulation model. Geomorphology 120, 195-208.

Texas Commission on Environmental Quality, 2008. Wind Roses 1984-1992. Web page: http://www.tceq.state.tx.us/compliance/monitoring/air/monops/windroses.html.

Thomas, D., Wiggs, G., 2008. Aeolian system responses to global change: challenges of scale, process and temporal integration. Earth Surface Processes and Landforms 33, 1396-1418.

Thomas, D., Knight, M., Wiggs, G., 2005. Remobilization of southern African desert dune systems by twenty-first century global warming. Nature 435, 1218-1221.

Thorpe, J., Wolfe, S., Houston, B., 2008. Potential impacts of climate change on grazing capacity of native grasslands in the Canadian prairies. Canadian Journal of Soil Science, 595-610.

Triantafilis, J., Lesch, S., 2005. Mapping clay content variation using electromagnetic induction techniques. Computers and Electronics in Agriculture 46, 203-237.

Triantafilis, J., Buchanan S., 2009. Identifying common near-surface and subsurface stratigraphic units with EM34 signal data and fuzzy k-means analysis in the Darling River valley. Australian Journal of Earth Sciences 56, 535-556.

USDA Soil Survey Staff, Natural Resources Conservation Service, United States Department of Agriculture. Web Soil Survey. Web page: http://websoilsurvey.sc.egov.usda.gov/.

Vance, R., Mathewes, R., Clague, J., 1992. 7000 year record of lake-level change on the northern Great Plains: a high-resolution proxy of past climate. Geology 20, 879-882.

Weight, R., Anderson, J., Fernandez, R., 2011. Rapid mud accumulation on the central Texas shelf linked to climate change and sea level rise. Journal of Sedimentological Research 81, 743-764.

Weaver, J., Zink, E., 1946. Annual increase of underground materials in three range grasses. Ecology 27, 115-127.

Weltje, G., Tjallingii, R., 2008. Calibration of XRF core scanners for quantitative geochemical logging of sediment cores: theory and application. Earth and Planetary Science Letters 274, 423-438.

Weymer, B., Everett, M., Houser, C., Wernette, P., Barrineau, P., 2016. Differentiating tidal and groundwater dynamics from barrier island framework geology: testing the utility of portable multifrequency electromagnetic induction profilers. Geophysics 81(5), E347-E361.

Wilkins, D., Currey, D., 1999. Radiocarbon chronology and $^{13}C$ analysis of mid- to late-Holocene aeolian environments, Guadalupe Mountains National Park, Texas, USA. The Holocene 9(3), 363-371.

Wolfe, S., Nickling, W., 1993. The protective role of sparse vegetation in wind erosion. Progress in Physical Geography 17(1), 50-68.

Wolfe, S., Ollerhead, J., Lian, O., 2002. Holocene eolian activity in south-central Saskatchewan and the southern Canadian Prairies. Geographie physique et Quaternaire 56, 212-227.

Wolfe, S., Ollerhead, J., Huntley, D., Lian, O., 2006.Holocene dune activity and environmental change in the prairie parkland and boreal forest, central Saskatchewan, Canada. The Holocene 16, 17-29.

Woodhouse, C., Overpeck, J., 1998. 2000 years of drought variability in the central United States. Bulletin of the American Meteorological Society 79(12), 2693-2714.

Wright, L., Short, A., Green, M., 1985. Short-term changes in the morphodynamic states of beaches and surf zones: an empirical predictive model. Marine Geology 62, 339-364.

Yu, J., Norwine, J., Bingham, R., Tebaldi, C., 2006. Potential climatic deterioration in semiarid subtropical South Texas. Web page: http://www.siue.edu/GEOGRAPHY/ONLINE/Yu06.doc.

# APPENDIX

## TABLES AND FIGURES

Table 1. OSL sampling scheme and results.

| Core Site | OSL Lab Number | Depth (m) | Aliquots[a] | U (ppm)[b] | Th (ppm)[b] | K (%)[b] | Cosmic dose rate (mGray/yr) | Dose rate (mGray/yr)[c] | OSL age[d] |
|---|---|---|---|---|---|---|---|---|---|
| 5 | BG4108 | 0.15 | 33/35 | 1.08 ± 0.01 | 2.66 ± 0.01 | 1.51 ± 0.01 | 0.19 ± 0.02 | 2.03 ± 0.10 | 75 ± 7 |
| 5 | BG4109 | 1.00 | 33/35 | 0.93 ± 0.01 | 1.94 ± 0.01 | 1.33 ± 0.01 | 0.17 ± 0.02 | 1.74 ± 0.09 | 4135 ± 300 |
| 8 | BG4106 | 0.15 | 33/35 | 0.79 ± 0.01 | 1.73 ± 0.01 | 1.32 ± 0.01 | 0.19 ± 0.02 | 1.70 ± 0.09 | 235 ± 20 |
| 8 | BG4107 | 1.05 | 33/35 | 0.73 ± 0.01 | 1.68 ± 0.01 | 1.30 ± 0.01 | 0.17 ± 0.02 | 1.64 ± 0.08 | 1935 ± 140 |
| 10 | BG4110 | 0.35 | 33/35 | 0.77 ± 0.01 | 1.89 ± 0.01 | 1.30 ± 0.01 | 0.19 ± 0.02 | 1.68 ± 0.09 | 230 ± 25 |
| 10 | BG4111 | 0.95 | 34/36 | 0.81 ± 0.01 | 2.52 ± 0.01 | 1.36 ± 0.01 | 0.17 ± 0.02 | 1.78 ± 0.09 | 6560 ± 460 |

[a] Aliquots used in equivalent dose calculations versus original aliquots measured

[b] U, Th, and K content analyzed by inductively-coupled plasma-mass spectrometry analyzed by ALS Laboratories, Reno, NV; U content includes Rb equivalent

[c] Assumes a moisture content of 3 ± 1 %

[d] Systematic and random errors calculated in a quadrature at one standard deviation. Datum year is AD 2010

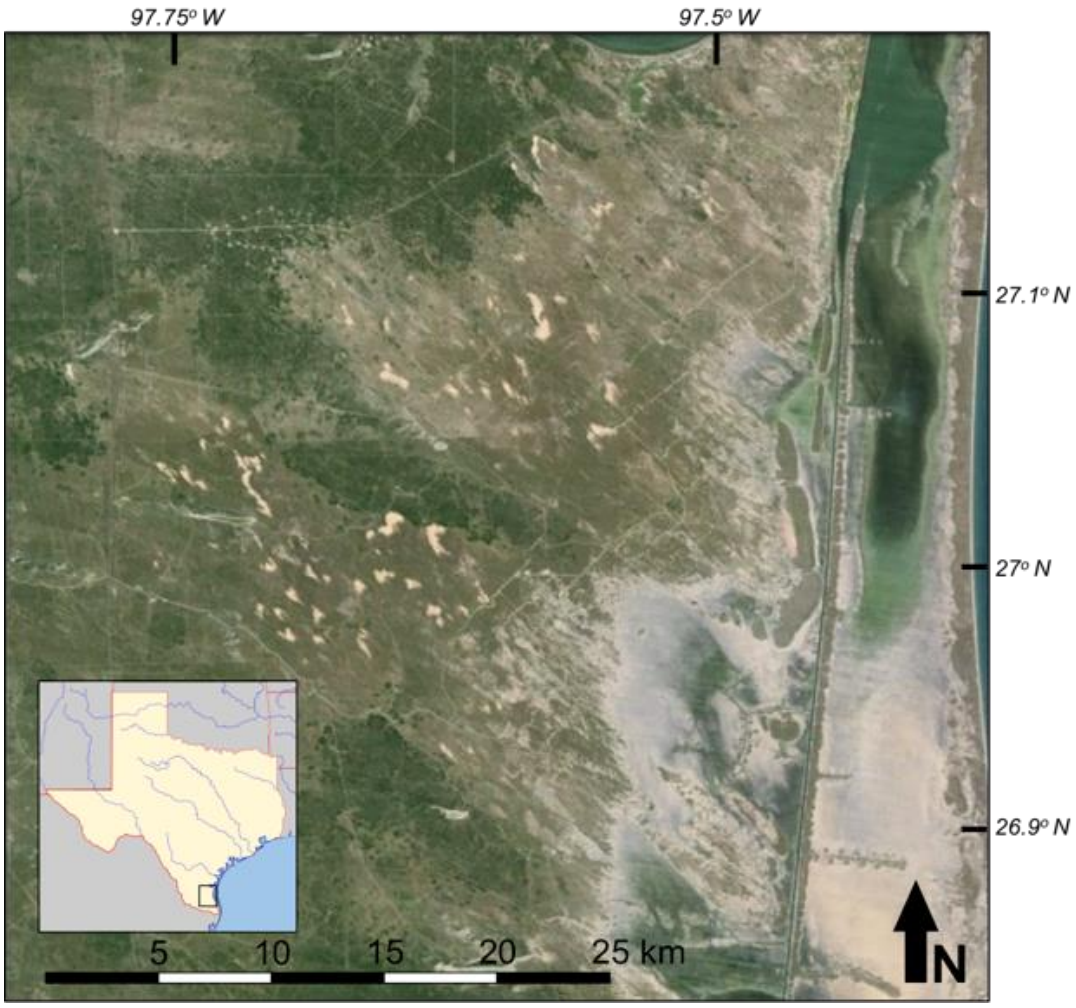


Figure 1. Study Area. Location within Texas shown as inset.

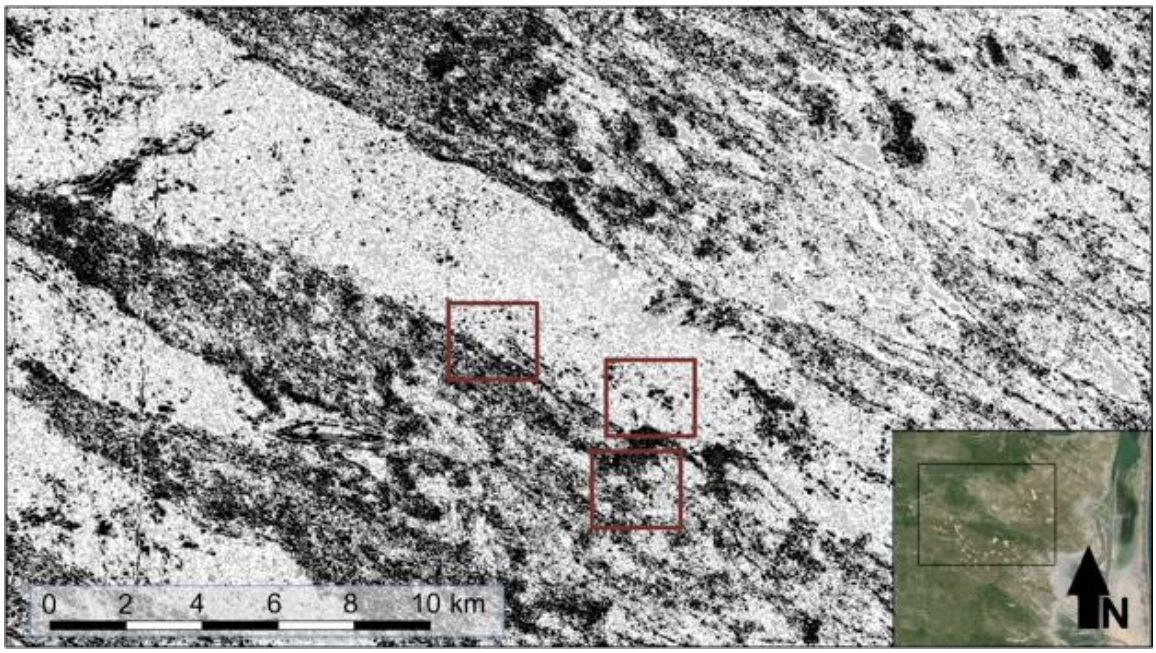


Figure 2. Classification of Principal Components. Darker shades of grey indicate more distinct aeolian morphometries; location within the region shown as inset. There are several phases of activity evident from this image. Focus areas 1, 2, and 3 are shown with maroon boxes.

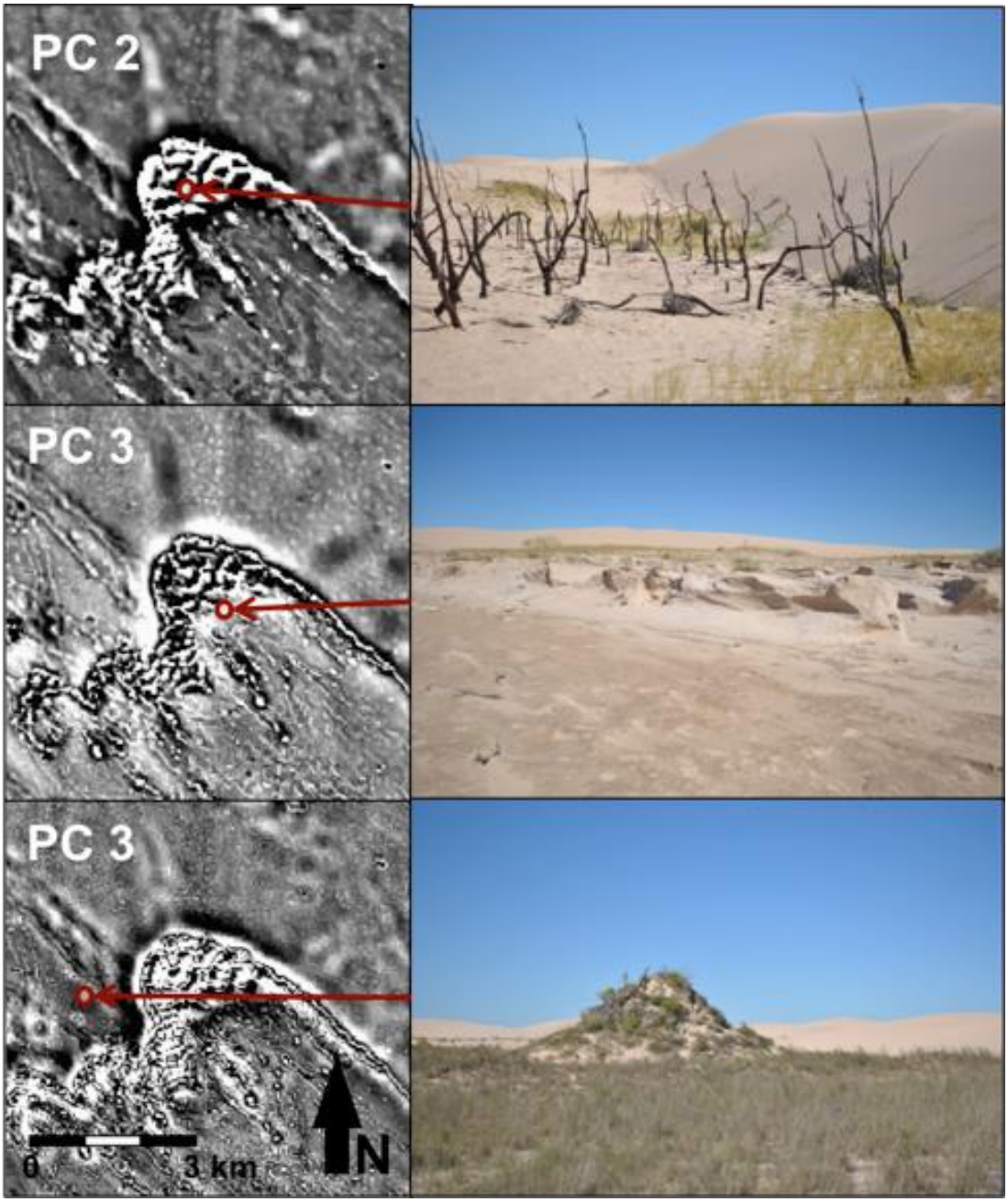


Figure 3. Components 1, 2, and 3.

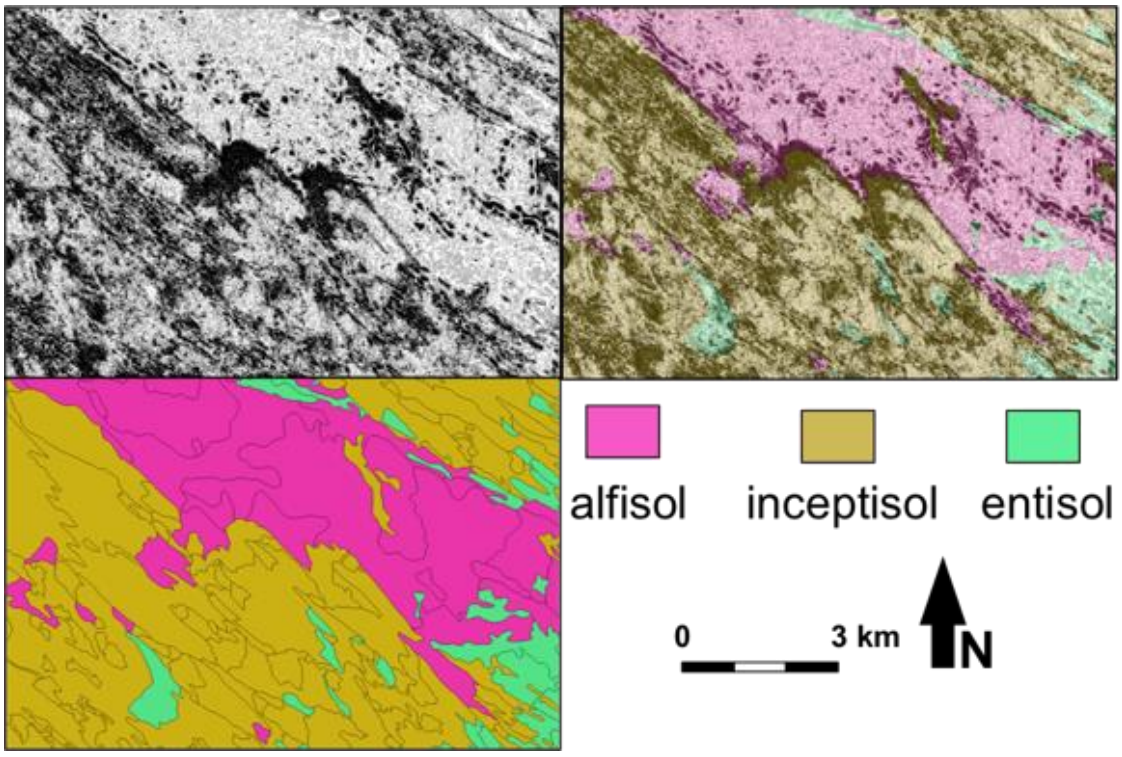


Figure 4. Soils and PC's 1, 2, and 3. Alfisols are the most developed, inceptisols are virtually undeveloped, and entisols are at an intermediate phase of horizonation. Notice the spatial relationship between patterning in the PCA classification and major soil orders indicating age elapsed since formation began.

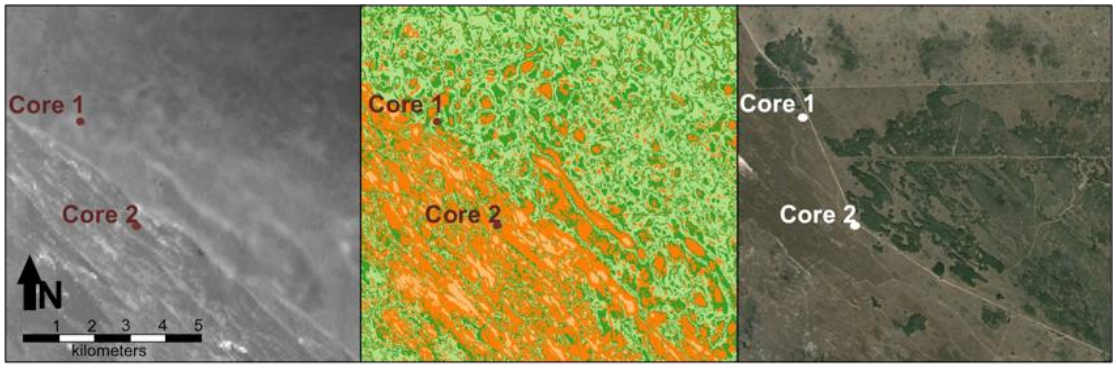

Figure 5. Cores 1 and 2 locations. Location of Cores 1 and 2 shown.

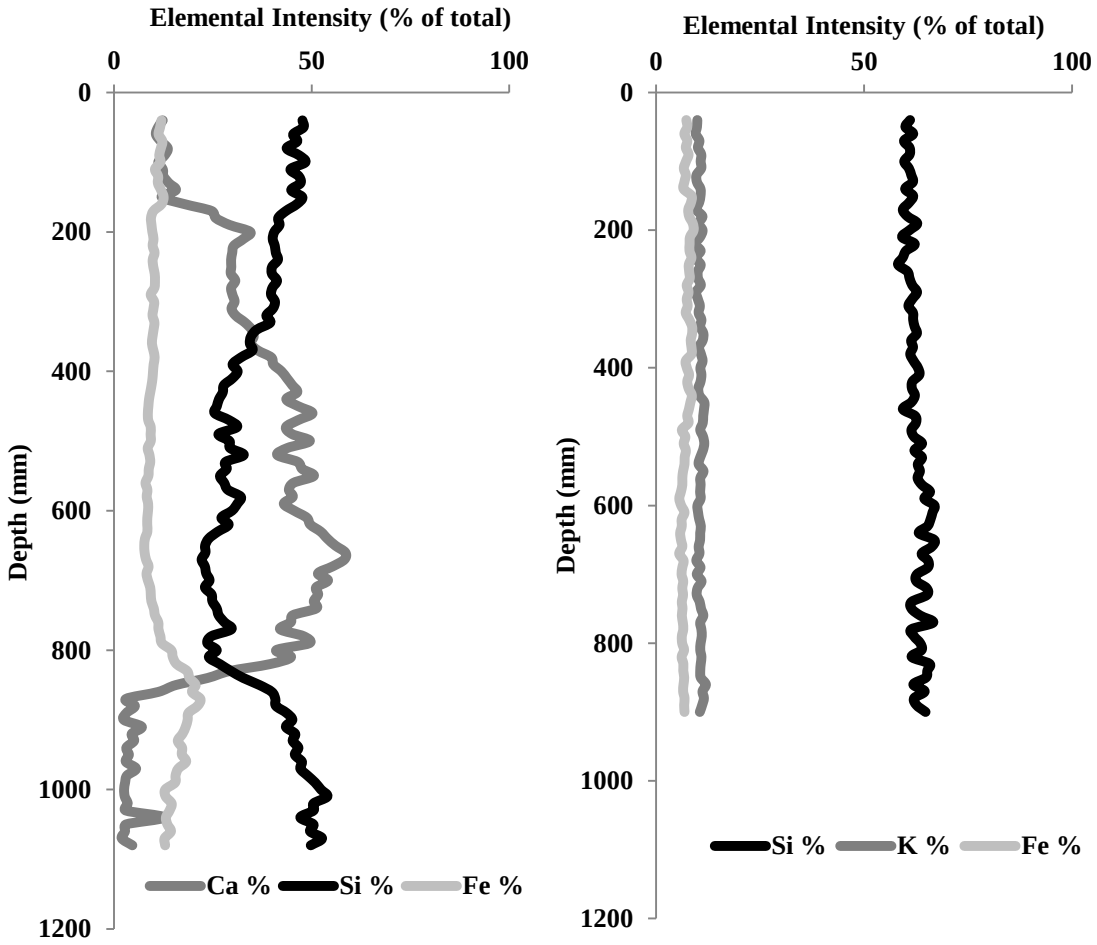

Figure 6. XRF results, cores 1 and 2

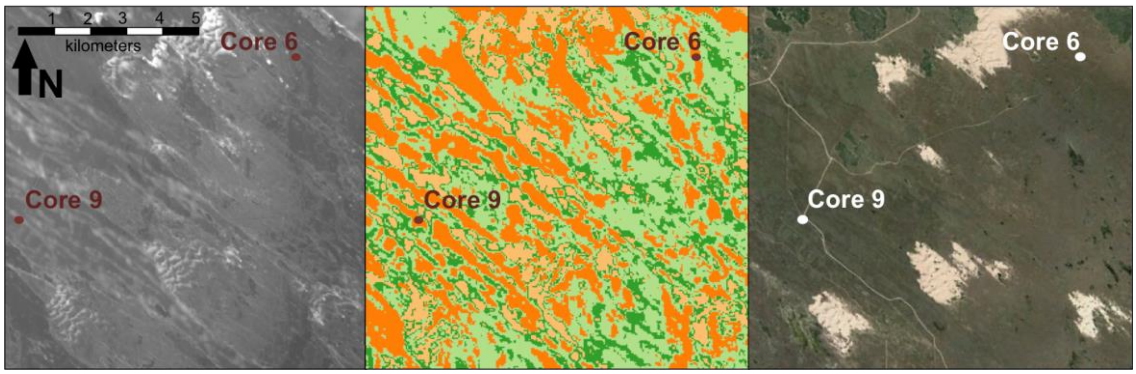

Figure 7. Cores 3 and 4 locations.

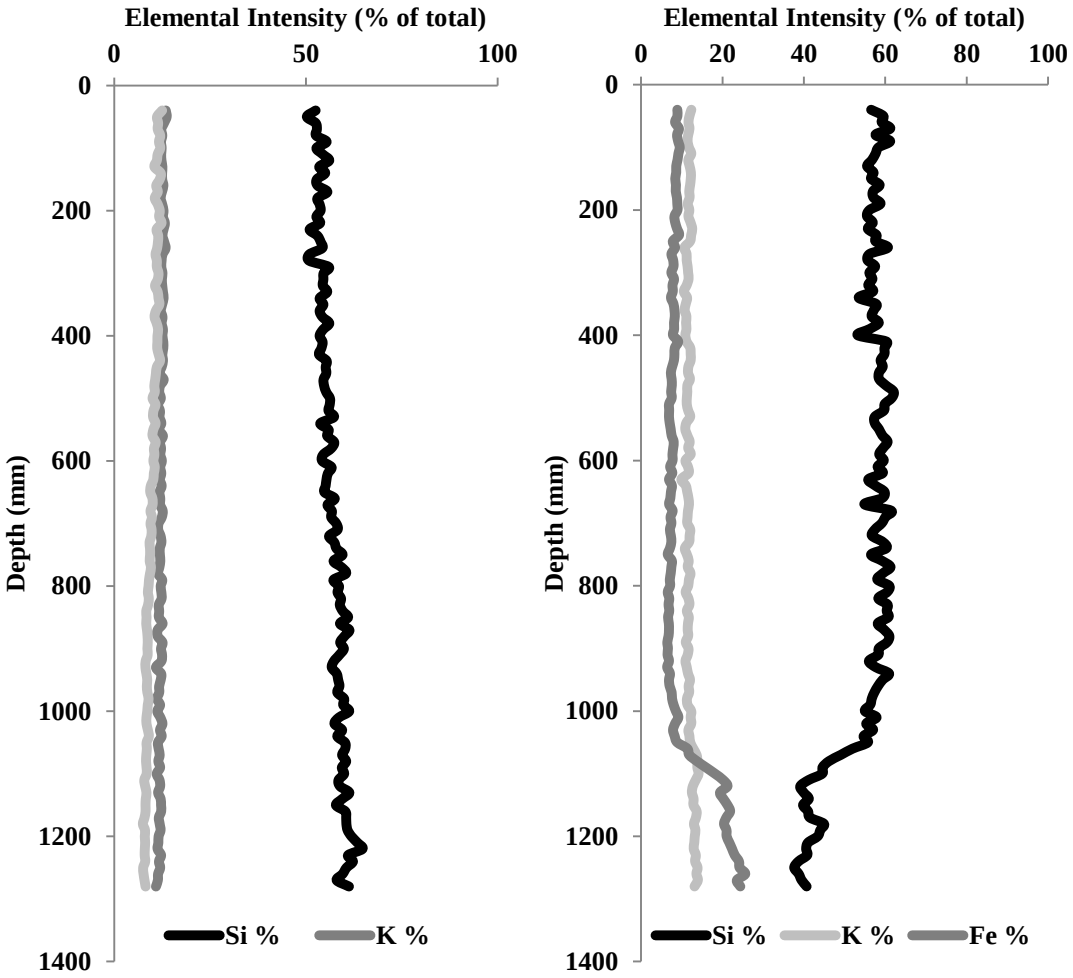

Figure 8. XRF results, cores 3 and 4.

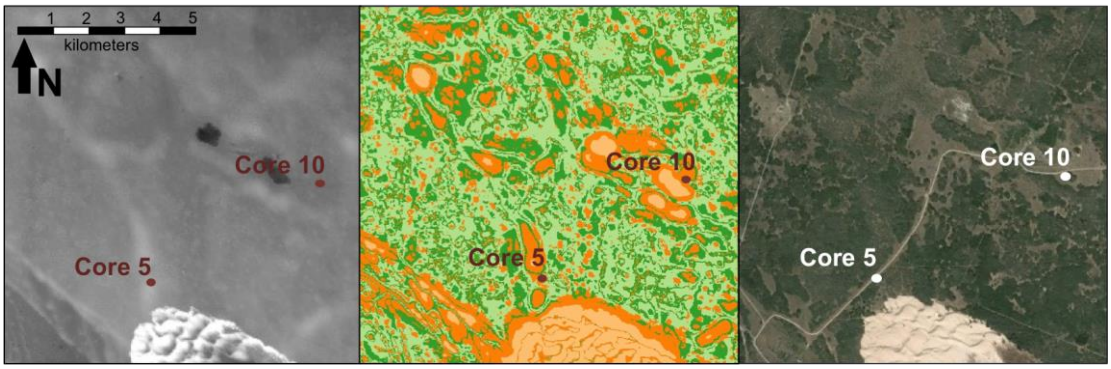


Figure 9. Cores 5 and 6 locations.

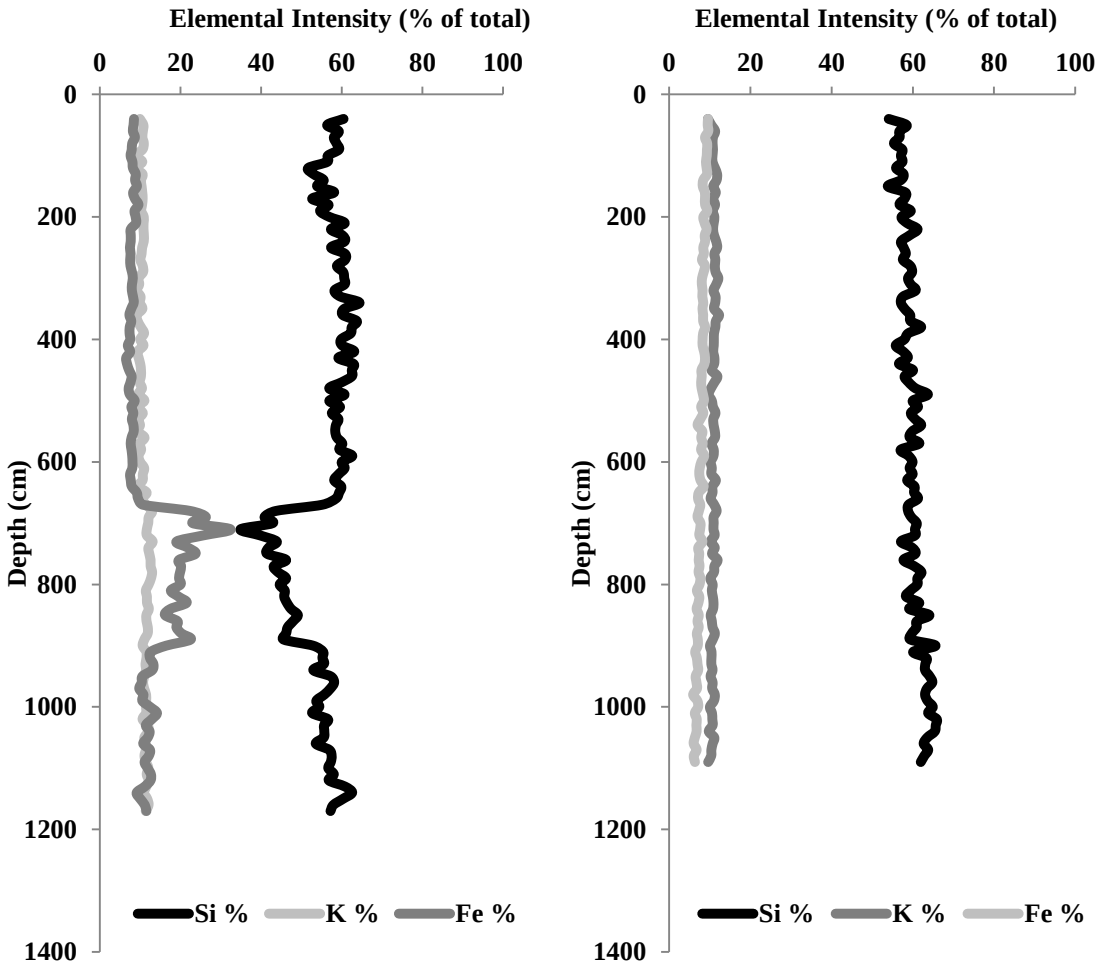


Figure 10. XRF results, cores 5 and 6.

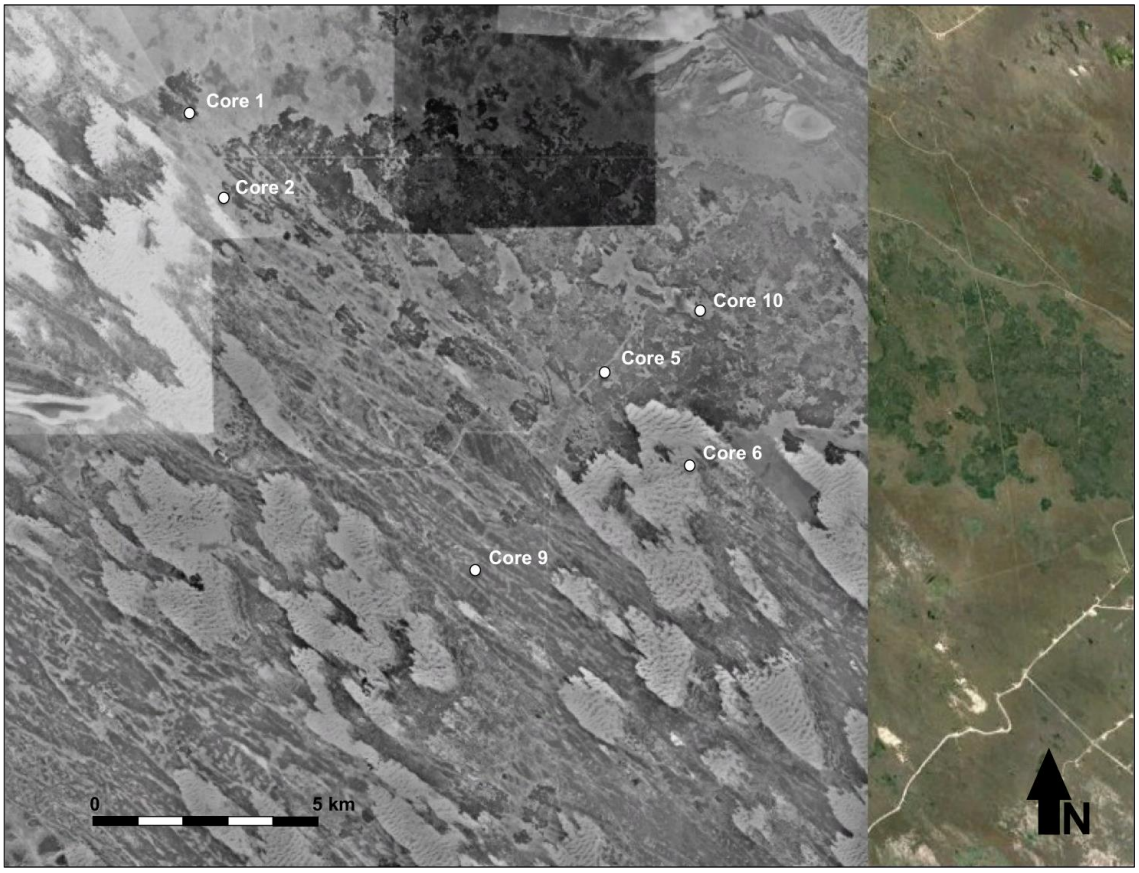


Figure 11. Study area, 1952.

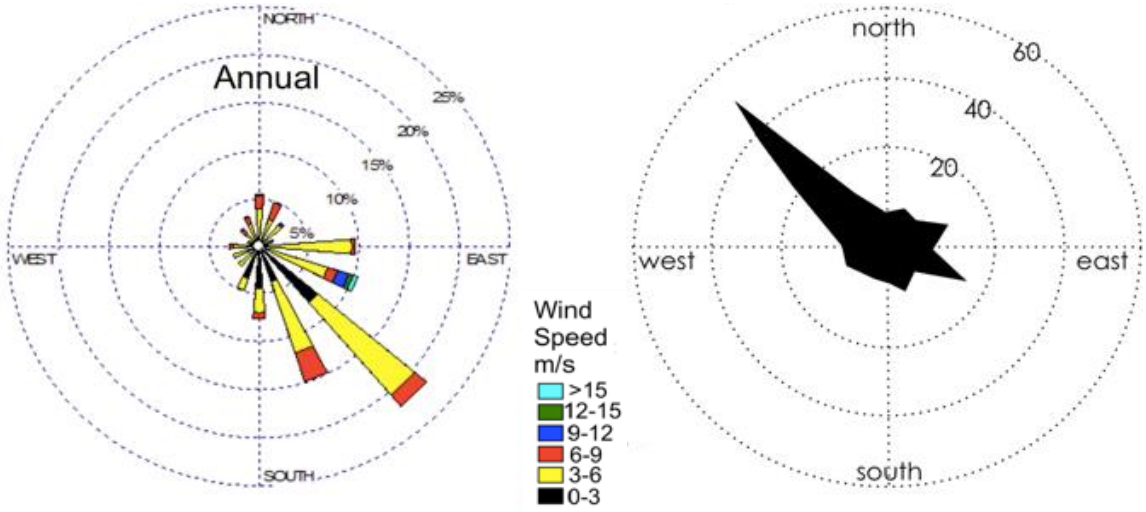


Figure 12. Wind rose and drift potential, South Texas (after Forman et al., 2009).

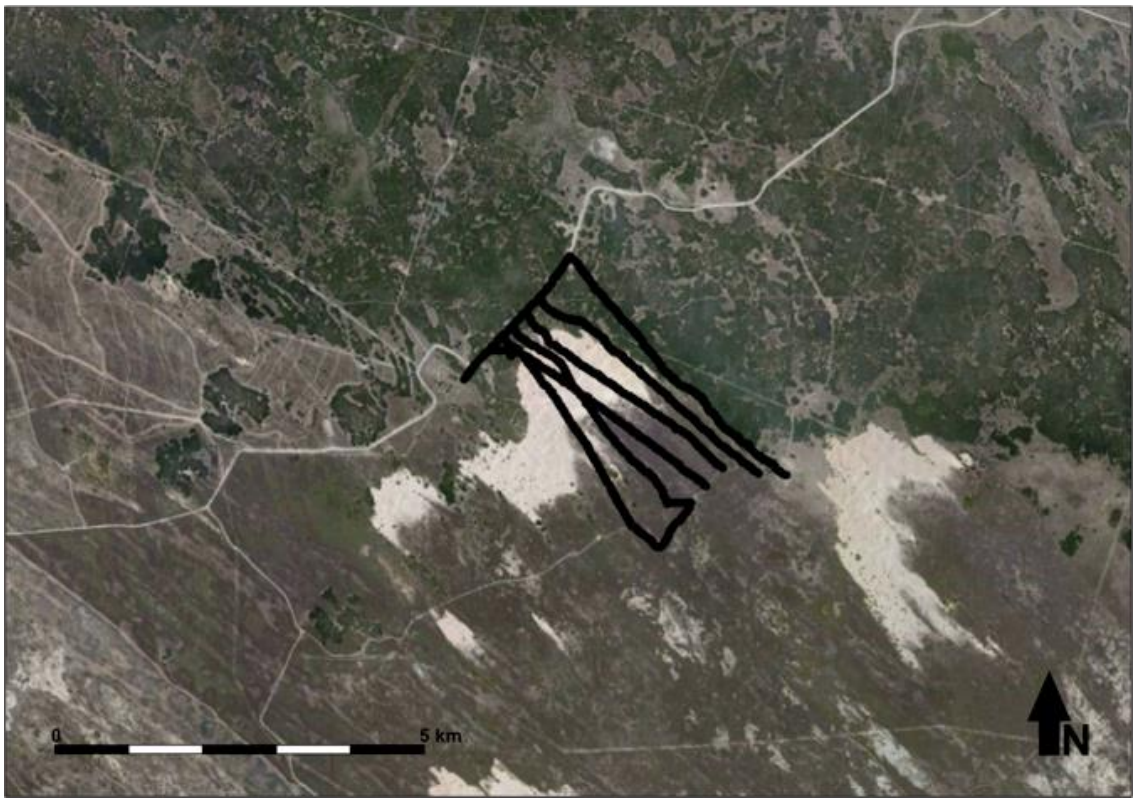


Figure 13. Electromagnetic survey lines.

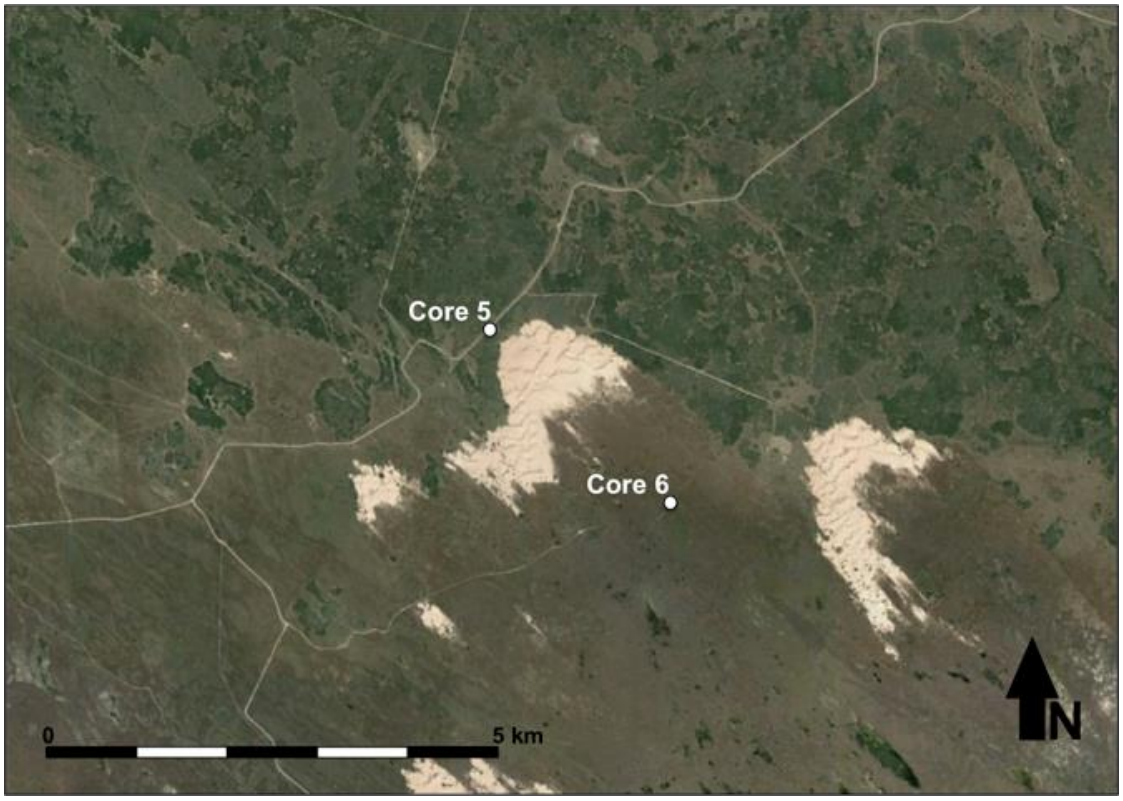

Figure 14. Cores 5 and 6 locations, close up.

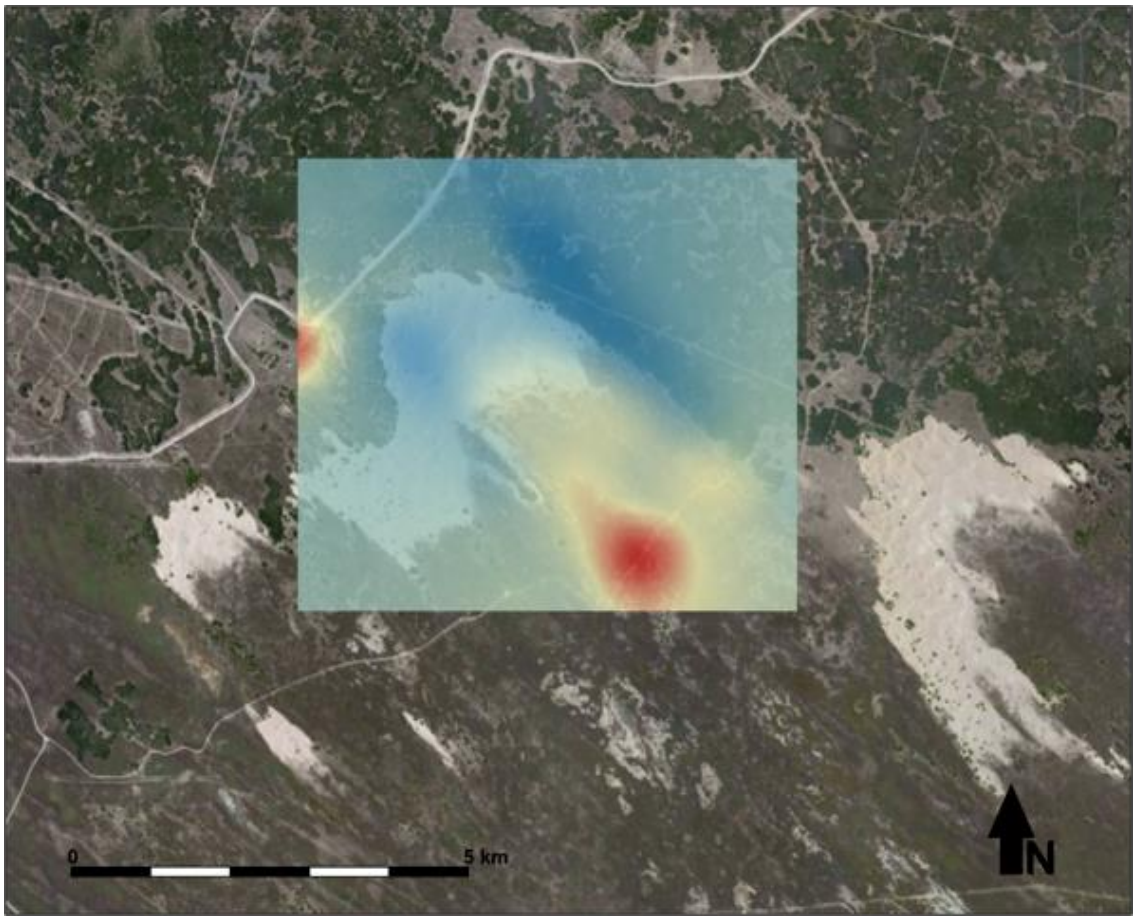

Figure 15. 15 KHz survey results. Higher apparent conductivities are shown in red, lower apparent conductivities are shown in blue.

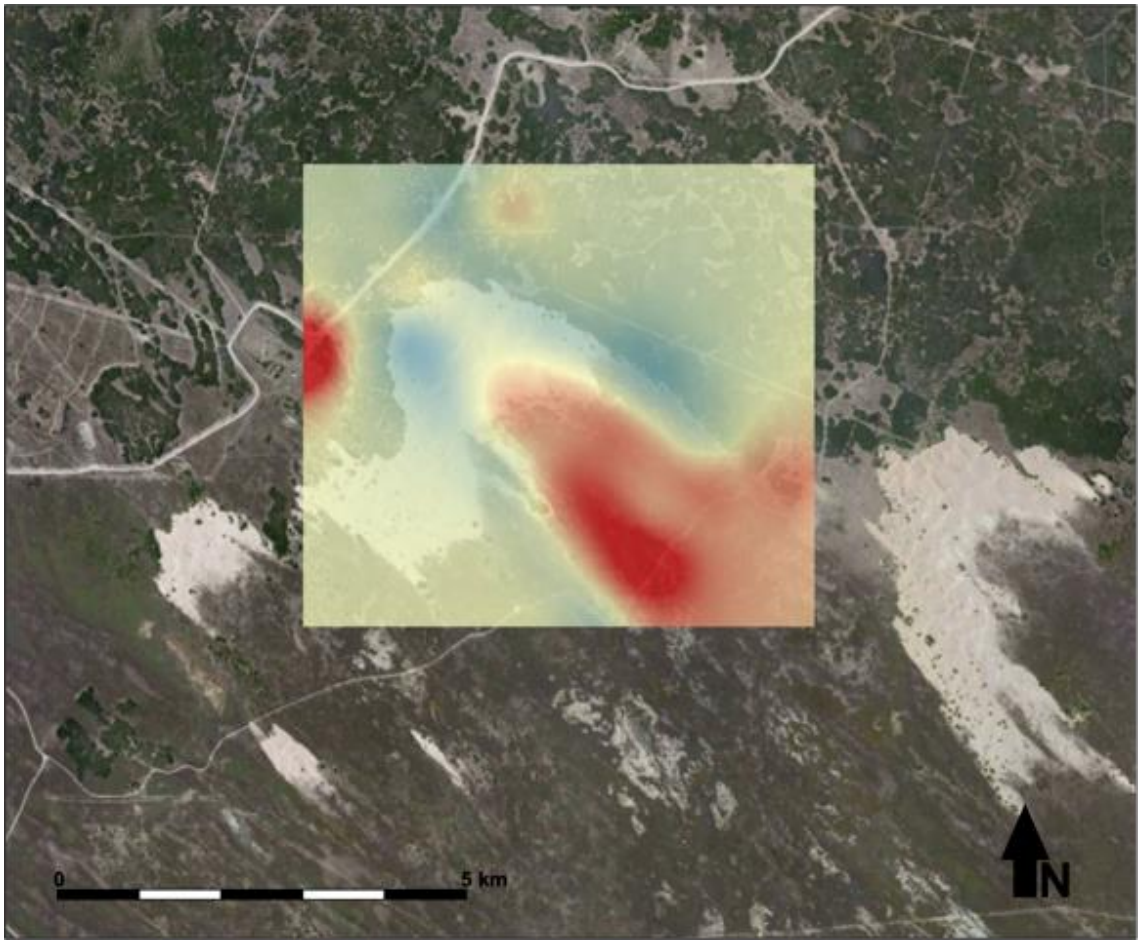


Figure 16. 5 KHz survey results. Higher apparent conductivities are shown in red, lower apparent conductivities are shown in blue.

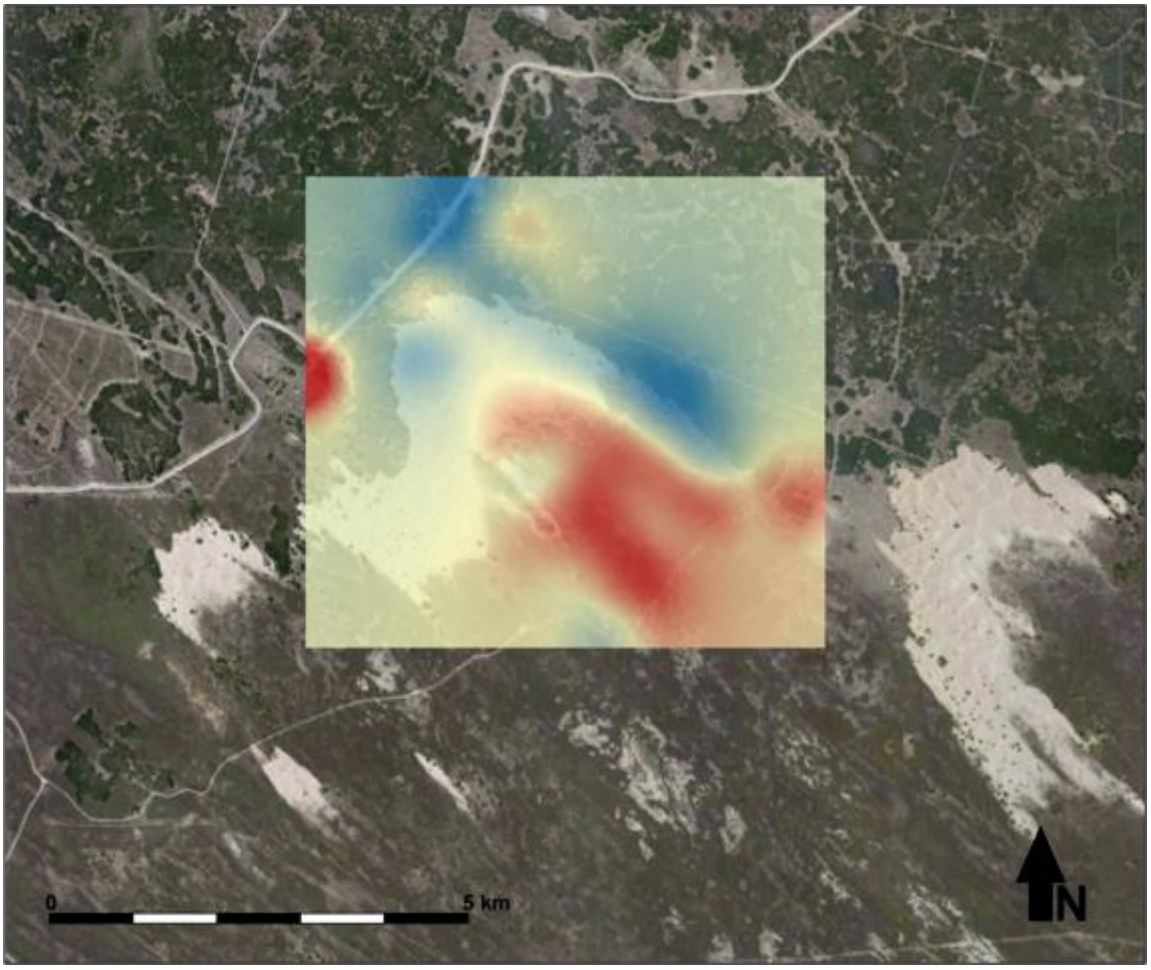


Figure 17. 3 KHz survey results. Higher apparent conductivities are shown in red, lower apparent conductivities are shown in blue.

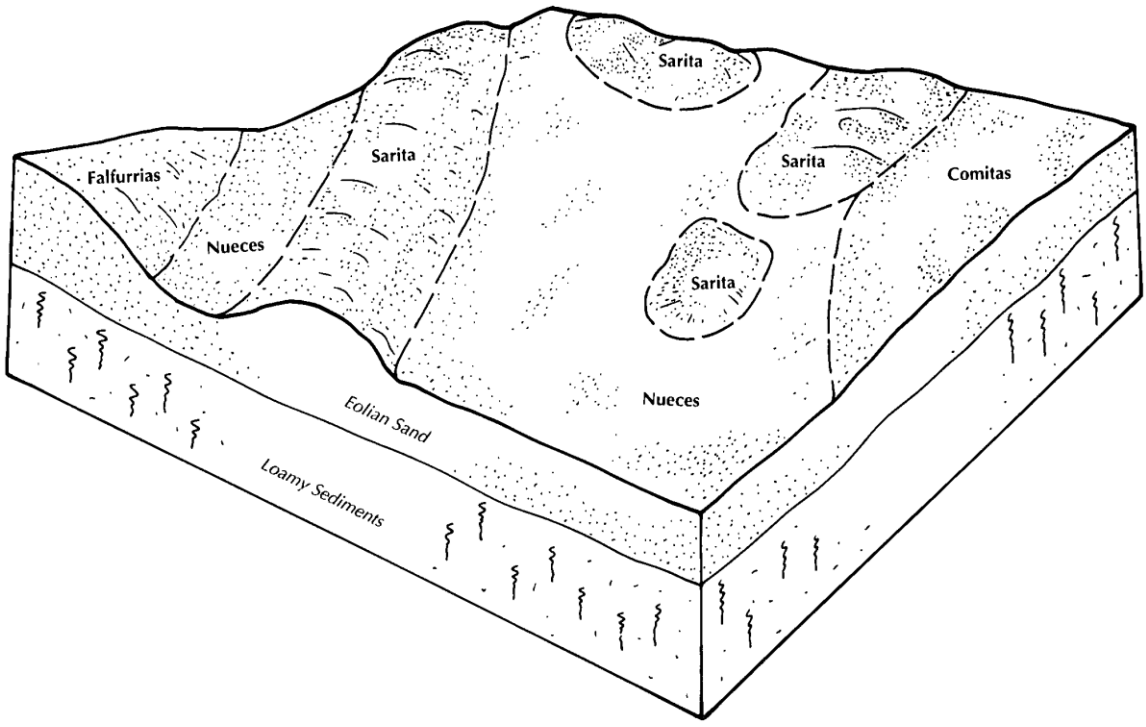


Figure 18. Conceptual soil block diagram.

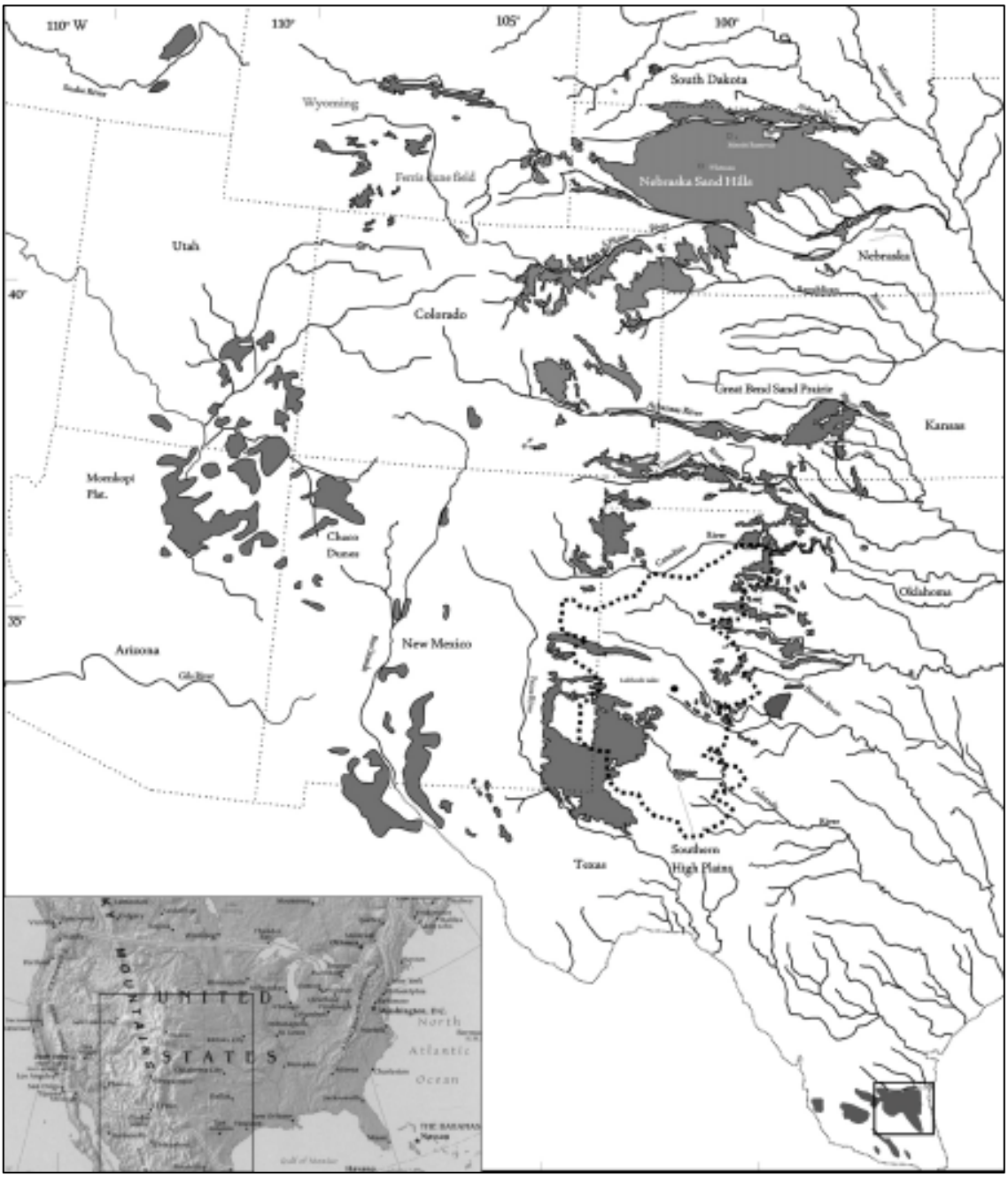

Figure 19. Dunes of the Great Plains. South Texas Sand Sheet in inset box (after Forman et al., 2009).

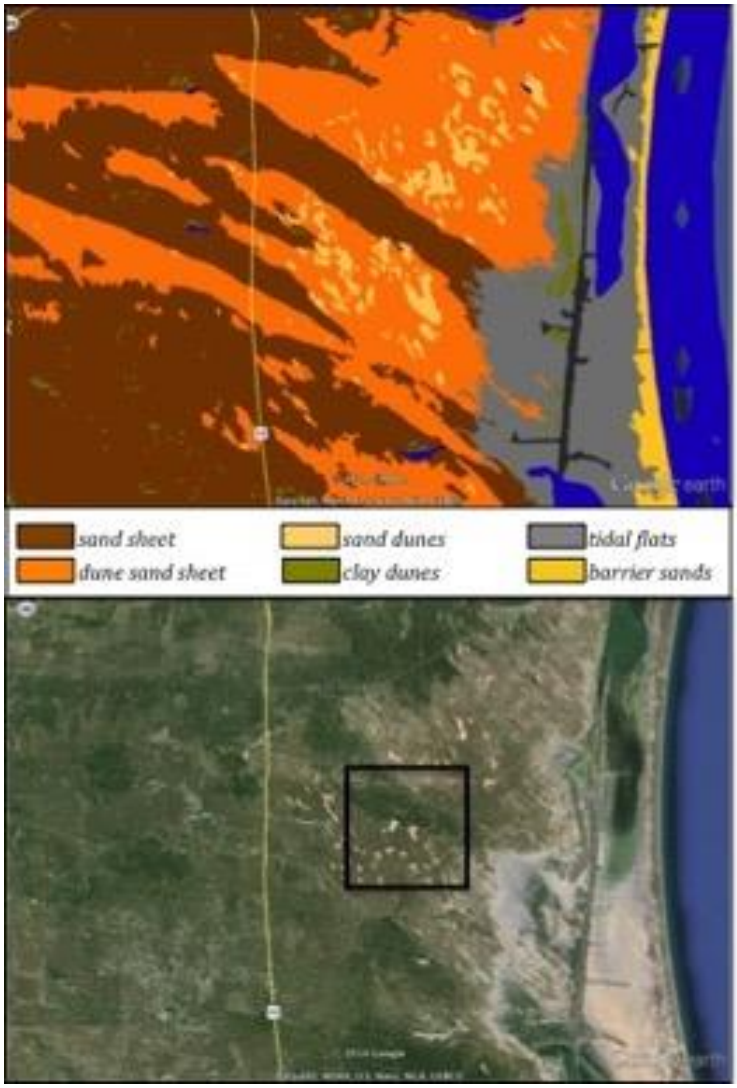


Figure 20. Soils of the South Texas Sand Sheet. Coring sample area located in inset box.

Figure 21. Core site locations.

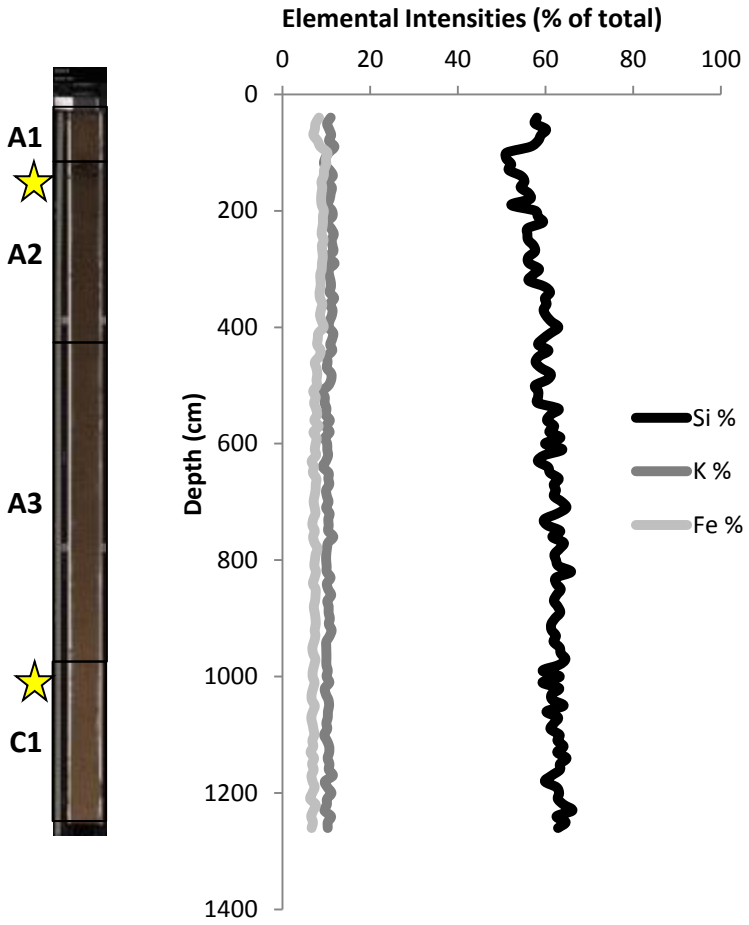


Figure 22. XRF results, core 5. Core 5 is a typic Falfurrias series entisol, shown with top three elemental intensities along with interpreted core image and location of OSL samples (shown with stars).

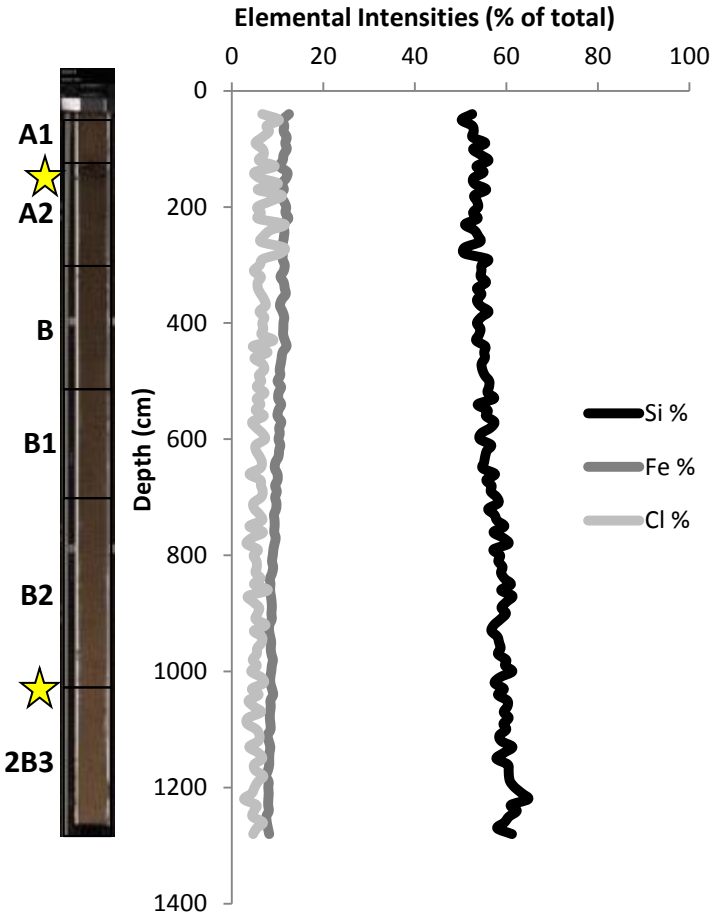


Figure 23. XRF results, core 8. Core 8 is a typic Nueces series alfisol, shown with top three elemental intensities along with interpreted core image and location of OSL samples (shown with stars).

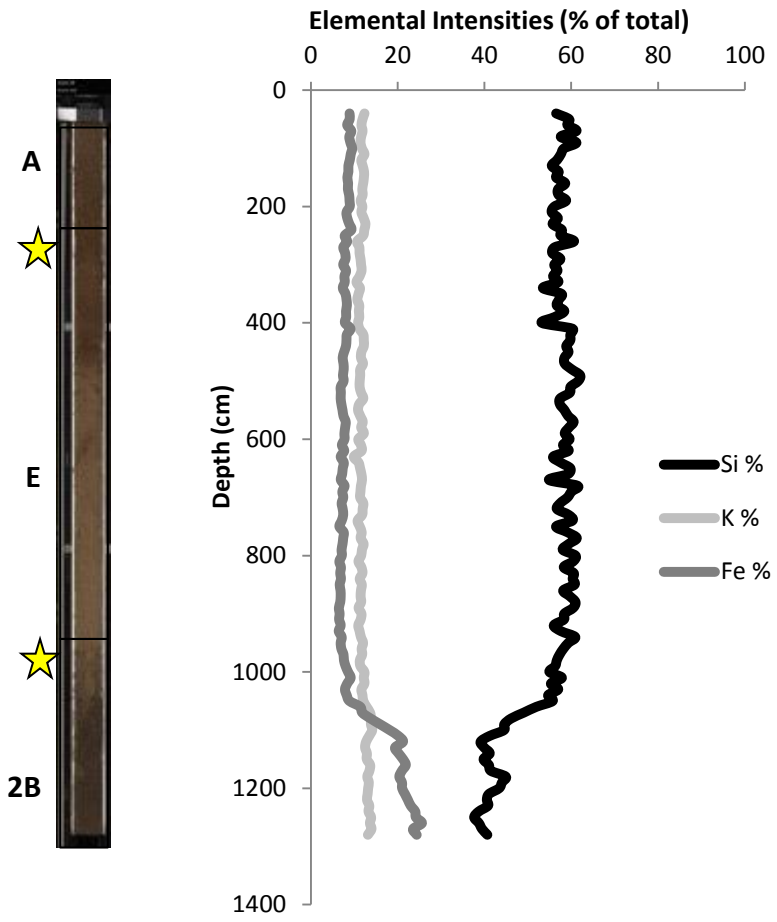


Figure 24. XRF results, core 10. Core 10 is a typic Sarita series alfisol, shown with top three elemental intensities along with interpreted core image and location of OSL samples (shown with stars).

Figure 25. Field photographs, core 5 and core 8. Core 5 (right), Core 8 (left).